

# ESAIL D4.6.2

## Simplified FEEP test report

Work Package: **WP 4.6**

Version: **Version 1.0**

Prepared by: Pierpaolo Pergola, Nicola Giusti, Salvo Marcuccio,  
Alta S.p.A.  
Time: Pisa, June 13th, 2013  
Coordinating person: Salvo Marcuccio, s.marcuccio@alta-space.com  
WP coordinator: Pierpaolo Pergola, p.pergola@alta-space.com

(List of participants:)

Participant no.	Participant organisation	Abbrev.	Country
1 (Coordinator)	Alta S.p.A.	Alta	Italy

## Table of Contents

0.	Scope.....	3
1.	Introduction .....	4
2.	Applicable documents .....	5
3.	Test main objectives.....	6
4.	Test description.....	7
4.1.	Test facility .....	7
4.2.	Thruster set-up .....	8
4.2.1.	The thruster assembly .....	9
4.2.1.1.	Thruster unit .....	9
4.2.1.2.	Thruster heaters and ground shield .....	11
4.2.1.3.	Propellant supply system.....	11
4.2.2.	Power control unit .....	13
4.2.3.	Beam diagnostic system.....	15
4.2.3.1.	Beam scan system.....	15
4.2.3.2.	Time of Flight system .....	16
4.3.	Preliminary operations.....	19
4.4.	Chamber preparation and setup integration .....	19
4.5.	Propellant outgassing.....	19
4.6.	Thruster bake out.....	19
4.7.	Dry insulation test .....	20
4.8.	Propellant pouring .....	20
5.	First test campaign results .....	21
5.1.	Onset voltage .....	21
5.2.	Current-Voltage characteristics.....	23
5.3.	Beam divergence angles .....	24
5.4.	Time of flight measurements .....	29
5.5.	Endurance test .....	34
6.	Second test campaign results .....	37
6.1.	Alternate voltage polarity mode.....	39
6.2.	Onset Voltage.....	41
6.3.	Beam divergence angles .....	42
6.4.	Time of flight measurements .....	43
6.5.	Thruster performance estimation .....	50
6.6.	Propellant consumption estimation .....	52

## **0. Scope**

This document summarizes the results of the experimental tests carried out, under the ESAIL FP7 project, on a linear slit FEEP emitter fed with the ionic liquid EMI-BF<sub>4</sub> as propellant.

## 1. Introduction

The Ionic Liquid FEEP (IL–FEEP) is a variant of the caesium–fed field emission thruster where the alkali metal propellant is replaced by ionic liquids.

Ionic liquids are organic molten salts composed of a mixture of loosely bound cations and anions, with the special property of being liquid at or close to room temperature. Such liquids have been developed by the chemical industry during the last 15 years for their unique properties as process fluids and solvents.

The usage of ionic liquids, with respect to alkali metals, leads to considerable simplifications in space and ground operations and the associated supporting equipment.

The possibility of contamination to the host spacecraft, as well as the danger of contamination of the thruster from the external environment, is much reduced.

In comparison to liquid metals, however, ionic liquid propellants have reduced performance in terms of specific impulse and mass efficiency.

In principle, operation in either pure ionic or mixed ion/droplet regime is possible, according to the choice of liquid and the operating conditions.

The IL–FEEP thruster design is based on the heritage of the classical Alta caesium FEEP.

## **2. Applicable documents**

AD-1: “Part B: Description of Work” of final EU E-sail application (final version)

AD-2: D4.6.1 Simplified FEEP design report (project deliverable)

AD-3. S. Marcuccio, N. Giusti, P. Pergola, "Ionic Liquid FEEP: Recent Experimental Results", 63rd International Astronautical Congress, Naples, Italy, IAC-12-A1-8-15, October 2012

AD-4: S. Marcuccio, N. Giusti, P. Pergola, "Development of a Miniaturized Electric Propulsion System for the E-Sail Project", 62nd International Astronautical Federation Congress, Cape Town, South Africa, IAC-11-B4-6A-3-x11311, October 2011

### 3. Test main objectives

The test campaign carried out aims at assessing the main characteristics of the ionic liquid FEEP thruster.

In particular, the test goals deals with the preliminary assessment of the following items (when possible in both positive and negative polarity and at different temperature values):

- thruster electrical parameters characterization:
  - onset voltage, i.e. the minimum voltage difference applied between emitter and accelerator to detect the ion emission,
  - tension-current (I-V) characteristics, i.e. the relation between the total voltage supplied to the thruster and the current that it generates in the beam,
- thruster beam characterization:
  - beam divergence angles, i.e. the half-angles encompassing the 97.5% of the beam in the two main orthogonal planes, see Figure 1,
  - beam composition, i.e. the spectrum of species (monomers, dimers, ..., droplets) composing the beam,
- thruster performance estimation:
  - propellant mass consumption,
  - specific impulse,
  - thrust magnitude.

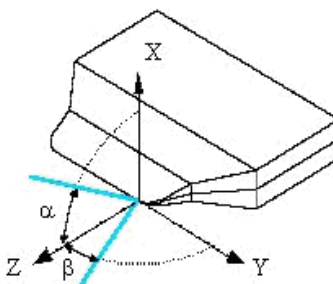


Figure 1: Definition of the beam divergence half angles

The threshold voltage value affects the size of the Power Control Unit (PCU), as the lower this value, the lighter the PCU system.

Moreover low thruster operating voltages reduce the issues concerning the electrical insulation making easier the implementation of the thruster on-board the Remote Unit.

I-V characteristic allows for identifying the working points required during the Remote Units flight operations.

The beam divergence angles are fundamental to assure that the thruster plume does not impact any physical surface and charged particles do not damage Remote Unit components. Any surface of the Remote Unit must be placed outside the thruster plume. The assessment of the beam divergence angles is performed by means of a scan system composed of two electrostatic single wire probes moving through the beam.

The thruster performance is affected by the species composing the beam. In case of only single ions compose the beam (pure ionic regime), the highest specific impulse and the lowest propellant consumption are obtained. On the contrary, large amount of droplets in the beam (ion-droplets mixed regime) determines lower specific impulses and larger propellant consumptions, but gives higher thrust magnitudes. The assessment of the beam composition is performed by means of the Time of Flight (ToF) technique, using simple targets in the first test campaign and a specific commercial device in the second.

## 4. Test description

In this chapter the main set-up items (the test facility, the thruster set-up, the beam diagnostic system, etc.) and the test phases (vacuum procedure, bake out of chamber and thruster, firing operations) are described.

The thruster characterization required two consecutive test campaigns. The first gave preliminary results and highlighted some experimental issues affecting the thruster performance. The second aimed at refining the preliminary results overcoming the problems arose in the first test campaign.

### 4.1. Test facility

Thruster emissions must be studied under conditions similar to those expected in space. However, because of the large difference in pressures between a vacuum chamber and the outer space, it is important to determine if non-ideal laboratory conditions affect experimental outcomes. If charged particles do not interact with the residual gas inside the vacuum chamber, it can be assumed that ground testing is representative of actual thruster operations. The best parameter to verify this situation is the mean free path of emitted particles, which is roughly proportional to  $1/nQ_c$ , with  $n$  the residual gas number density and  $Q_c$  its collision cross section. Assuming an ideal gas,  $Q_c = 3 \cdot 10^{-19} \text{ m}^2$  (relatively large residual molecules) and a minimum mean free path of 3 m, the pressure inside the vacuum chamber must be below  $4.7 \cdot 10^{-5} \text{ mbar}$  to avoid gas-particle interaction.

The test campaigns were carried out in two different vacuum facilities:

- a cylindrical vacuum chamber with an inner diameter of 0.6 m and a length of 1.5 m, see Figure 2, for the first test campaign
- a cylindrical vacuum chamber with an inner diameter of 0.5 m and a length of 1.0 m in length was used, see Figure 3, for the second test campaign

The two chambers are equipped with similar vacuum pumping systems, both composed of a rotary pump (120 l/min pumping speed) for low vacuum ( $10^{-2} \text{ mbar}$ ) and a turbo-molecular pump (500 l/sec pumping speed) high and ultra-high vacuum ( $10^{-8} \text{ mbar}$ ).

The ultimate vacuum maintained during tests during thruster operation was of  $10^{-6} \text{ mbar}$ .

Similar measurement and automation systems are available on both chambers.

The small volume difference between the two facilities did not significantly affect the ionic liquid FEEP thruster operations.

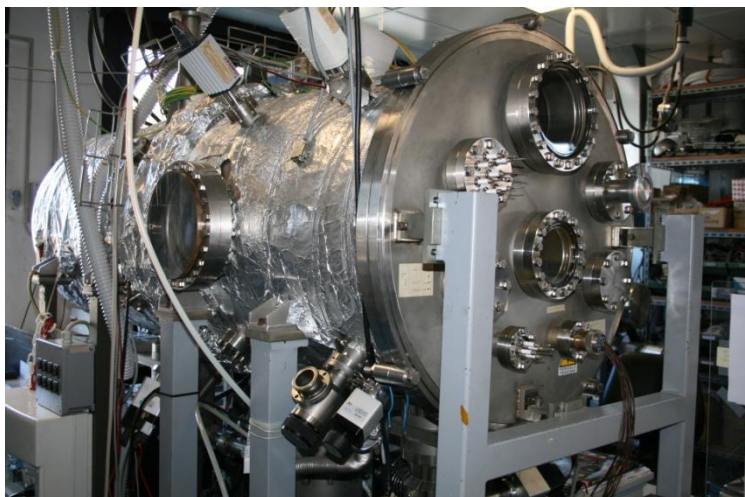


*Figure 2: Facility used for the first test campaign*

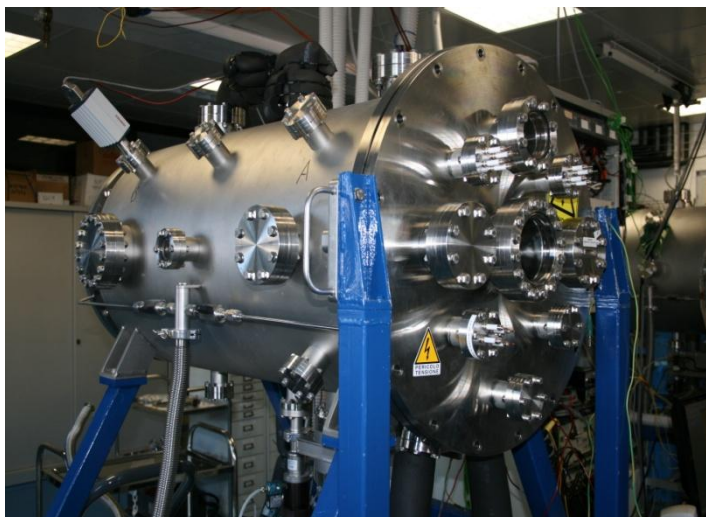


*Figure 3: Facility used for the second test campaign*

During tests all the relevant data were collected by means of the laboratory acquisition system:

- the analogue signals (vacuum chamber pressure, temperature values and thruster electrical parameters) and the digital I/O signals for the facility control were managed with a distributed I/O system operating at 1 Hz;
- the beam scan measurements were acquired by means of one NI PCI 6036e DAQ board (maximum sample rate of 200 kS/s),
- the ToF measurements were performed by means of one Tektronix DPO4104B oscilloscope (maximum sample rate 5 GS/s).

## **4.2. Thruster set-up**

The thruster set-up used for the test campaigns includes

- thruster assembly,
- power control unit,
- beam diagnostic system.

These items are detailed in the following paragraphs.

### 4.2.1. The thruster assembly

The thruster assembly includes

- the thruster unit, composed of the electrodes (emitter unit and accelerator), the insulators of the two electrodes and the high voltage cables and connections,
- the thruster unit heaters, used to perform the emitter unit bake-out and for varying the temperature (from room value up to 120 °C) during thruster characterization,
- the ground shield, i.e. a case protecting the electrodes from electrostatic interferences,
- the propellant supply system, composed of the feeding system, i.e. the propellant reservoir and duct, and the pouring system, designed to refurbish the propellant consumed during operation.

Figure 4 shows the thruster assembly and the beam scan system before the integration in the vacuum chamber.

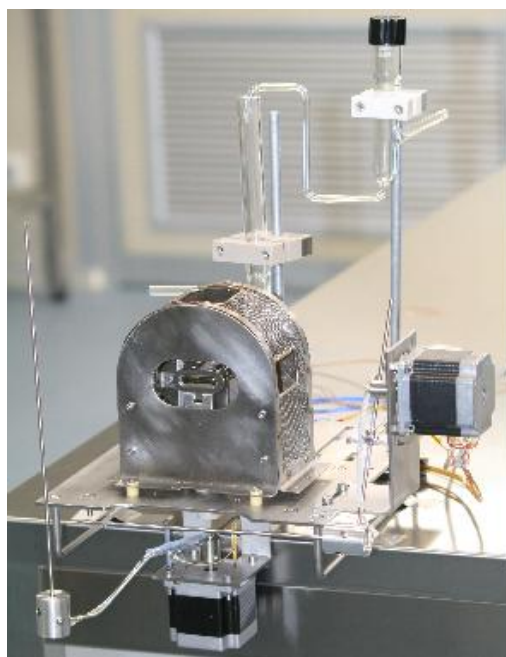


Figure 4: Thruster assembly and beam scan system

#### 4.2.1.1. Thruster unit

The thruster unit is composed of the linear slit emitter, the accelerator, the PEEK insulators and the HV cables.

The design of the emitter units used for the test campaign with the ionic liquids is the same of the cesium FEEP thruster. The overall emitter unit dimensions are 12x17x27 mm.

The emitter is manufactured in Inconel X750. It is composed of two half emitters, male and female. The female half-emitter is spattered with a nickel deposition of 1.5 micron. This deposition is shaped so as to realize the propellant duct when the two half-emitters are coupled. The linear slit is 8 mm in length.

The management of the emitter was performed following the procedures developed for the cesium FEEP flight program in the ISO5 cleaning room available at Alta's premises.

The inspection of the two half emitters was carried out to verify that the two blades were free of macro-defects, which might determine anomalous emission sites.

After the inspection, the half-emitters were coupled under an optical microscope to match

the high precision requirements on the alignment.

A set of M2 screws are used for tightening the unit to avoid propellant leakage along the external boundary.

To verify the sealing effectiveness, a bubble leak test was performed, see Figure 5. The test highlighted a uniform bubble path along the slit region and no leakage outside.

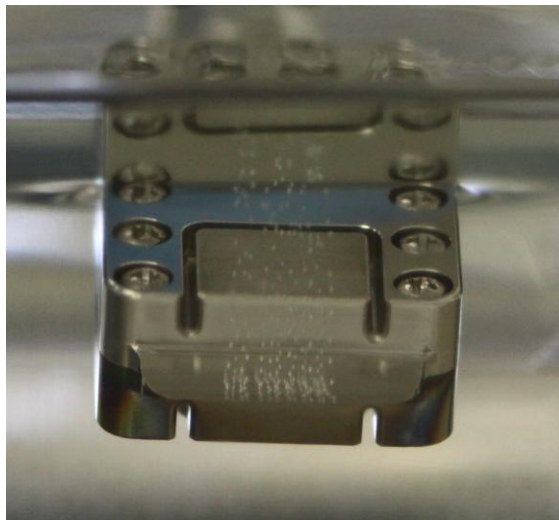


*Figure 5: Bubble test of the emitter unit*

Two different units have been used in the two test campaigns as after each test the emitter always shows degradation that might affect further usage. The two units were similar for geometric characteristics and blade precision.

The accelerator is a stainless steel plate with a countersunk rectangular (rounded edges) crevice 4 mm in height. The same accelerator has been used in the two test campaigns.

In the same fashion of the emitter unit, also the accelerator was inspected under the optical microscope to verify that the blade did not present any defect.

A picture of the accelerator on its support before the assembly in the vacuum chamber is shown in Figure 6.



*Figure 6: Accelerator close up during the thruster system integration.*

The typical voltage difference applied between the emitter and the accelerator electrode is around 10 kV. The electrical insulation between electrodes and the ground was guaranteed by means of simple PEEK insulators cylindrical in shape ( $\phi=30$  mm,  $h=50$  mm).

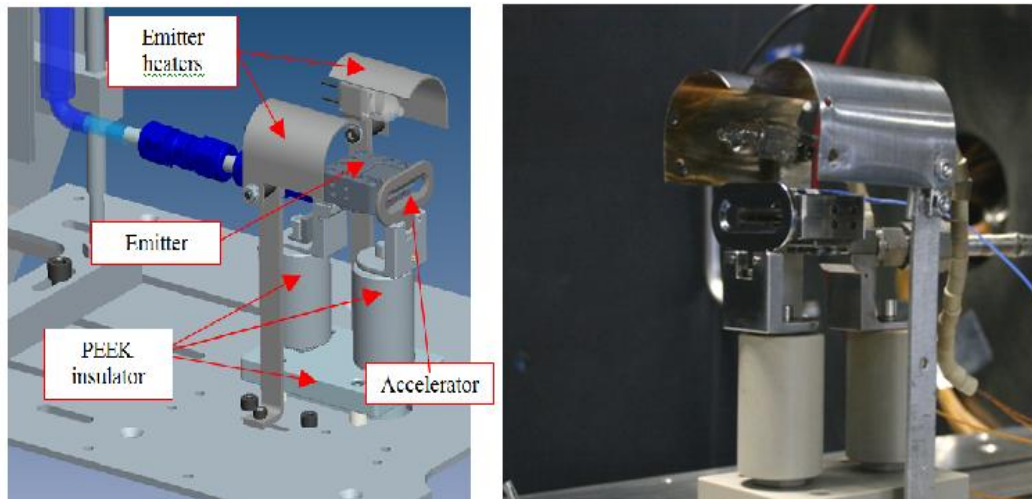


Figure 7: Thruster unit

#### 4.2.1.2. Thruster heaters and ground shield

Two heaters (50 W halogen lamps) placed on the two sides of the emitter were used to perform the bake-out of the unit. The bake-out was performed maintaining the emitter unit at 100°C for 48 hours (14.4 W of total power for the two heaters).

Moreover the heaters were also used to investigate the thruster behavior at different temperatures, in particular the tests were carried out at the following temperatures:

- room temperature (22-24°C),
- 40°C (heaters power 6.5 W),
- 60°C (heaters power 8.6 W),
- 80°C (heaters power 11.4 W),
- 100°C (heaters power 14.4 W),
- 120°C (heaters power 16.0 W).

During the thruster operation the emitter temperature was monitored by a fiber optic temperature sensor (FISO Technologies Inc.) placed on the male half-emitter.

The thruster unit shield is a grounded box of stainless steel, see Figure 9 and Figure 10. The case encompasses completely the two electrodes leaving only an elliptic window in front of the thruster unit for the beam emission.

Two additional windows, one on the right side and one on the top are left for the visual observation of the emitter during tests.

The same case has been used in both test campaigns.

#### 4.2.1.3. Propellant supply system

As per AD-2, the propellant used in both test campaigns is the 1-Ethyl-3-methylimidazolium tetrafluoroborate supplied by Sigma Aldrich. The main properties of the propellant are:

- abbreviation: EMI-BF<sub>4</sub>,
- CAS number: 143314-16-3,
- empirical formula (Hill Notation): C<sub>6</sub>H<sub>11</sub>BF<sub>4</sub>N<sub>2</sub>,
- molecular weight: 197.97,
- mass anion: 86.77 amu,
- mass cation: 111.200 amu,
- melting point (theoric): 15°C,

- density (theoric): 1218 kg/m<sup>3</sup>,
- electric conductivity: 1.4 S/m,
- surface tension: 0.0452 N/m,
- viscosity: 0.038 Pa·s.

The propellant supply system consists of the feeding system, i.e. the propellant reservoir and ducts, and the pouring system, designed to refurbish the propellant consumed during operation. All feeding system components are made in Pyrex, to allow for the visibility of the propellant head, besides the emitter side connection realized with glass-metal Swagelok tube fittings.

The two systems are required for two reasons:

- the liquid propellant requires an out-gassing process to removed the bulk gas (air) dissolved within the liquid itself,
- the emitter unit has to be fed with the propellant in vacuum conditions; otherwise the gas (air) trapped between the slit micrometric channel and the liquid meniscus blocks the propellant feeding to the slit itself (even weeks might be required to out-gas the internal volume of the emitter from the slit).

Two different pouring systems were used in the two test campaigns. In the first one an argon pressurized system was adopted.

The reservoir was manually filled before the chamber integration and once in vacuum the pressurization system spilled the propellant into the feeding system, see Figure 8 and Figure 9.

Some difficulties arose with this system for the control of the propellant spilling, thus in the second test campaign, a different pouring system was adopted.

The upper reservoir was manually managed by a rotative feed-through and the propellant spillage was controlled more precisely, see Figure 8 and Figure 10.

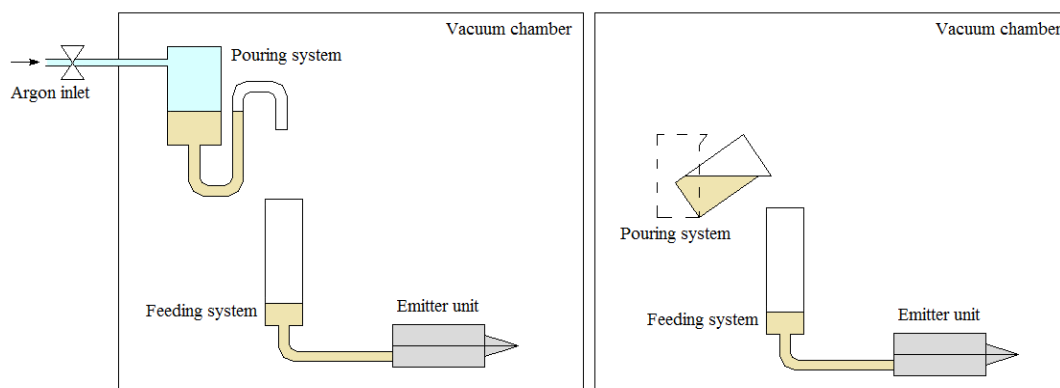
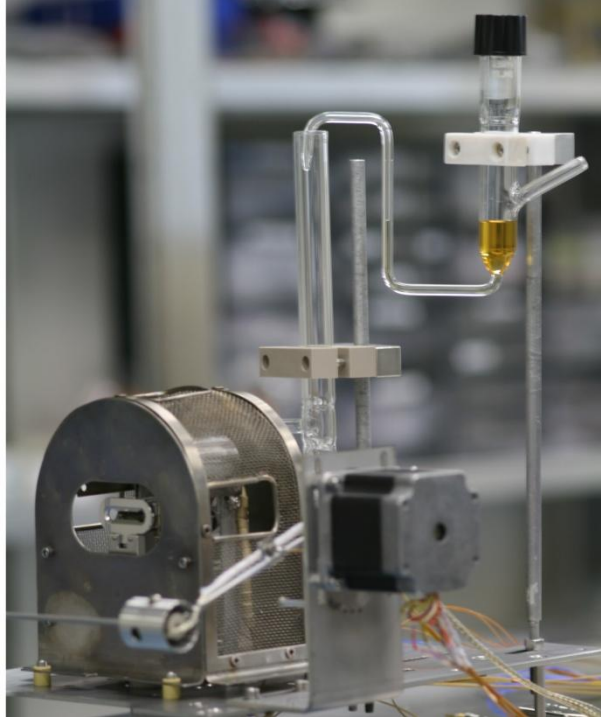
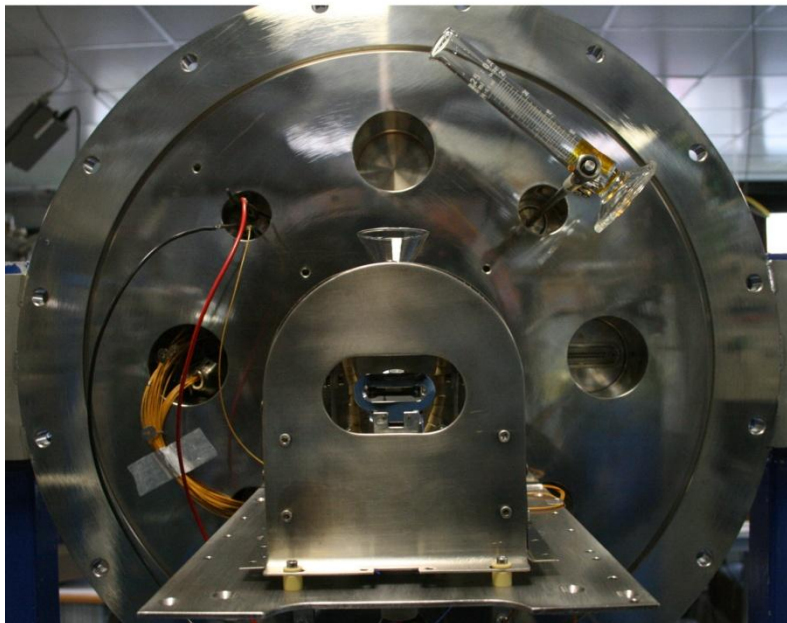


Figure 8: Propellant supply system sketch for the first test campaign (left) and for the second one (right)

The propellant spillage in the feeding system was carried out after the gas dissolved in the ionic liquid was completely released, to avoid bubble formation in the feeding duct.



*Figure 9: Feeding system used during the first test campaign*



*Figure 10: Feeding system used during the second test campaign*

#### **4.2.2. Power control unit**

Two different thruster power supply units have been used for the two test campaigns.

In the first case one commercial high voltage PCU, FuG HCP 140-12500, was used. This is the same model used for the development of the cesium FEEP. It operates with a voltage range 0-12.5 kV, a current range of 0-10 mA and allows for a switching frequency between positive and negative polarity of the order of 0,1 Hz.

For the second test campaign, instead, a dedicated PCU has been developed with the primary goal of increasing the thruster voltage switching frequency and better fitting with the ionic liquid thruster needs. A rough mock-up has been developed and tested in this WP.

The PCU developed is based on a commercial DC/DC converter (EMCO F-101). This device works with an input tension between 0 and 15 V and returns tensions between 0 and 10 kV allowing for currents up to 1 mA (10 W max power). This high voltage range is the one required to have the current lab prototype thruster firing.

The mock-up realized uses two EMCO modules and two high frequency and high voltage reed relays (Cynergy3 DAT72415R). These switches are used in Military and Defence systems and have been tested for Bump, Shock and Vibration endurance to the following standards:

- Bump Test: EN60068-2-29:1993 (Or Equivalent), 40g 6ms Pulse Duration,
- Shock Test: MIL-STD-202G (Or Equivalent), 100g 6ms Pulse Duration,
- Vibration Test: MIL-STD-202G (Or Equivalent), 20g 5-500-5Hz.

The electric circuit of the module is shown in Figure 11 together with a picture of the mock-up realized, see Figure 12.

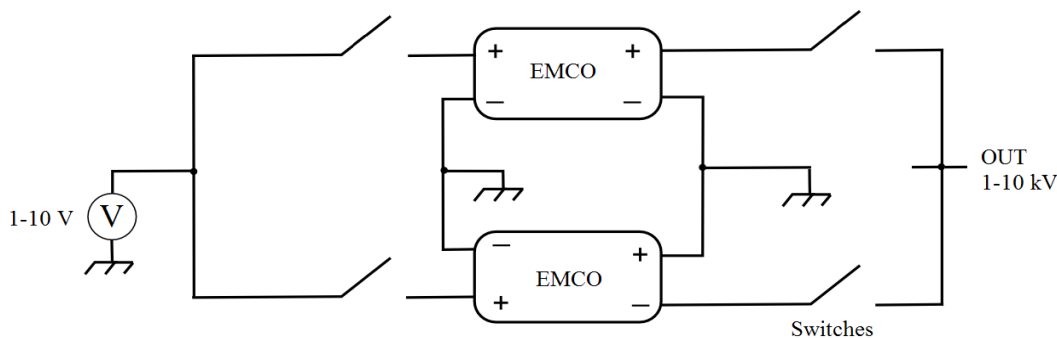


Figure 11: Double EMCO/2 HV switches PCU electric scheme

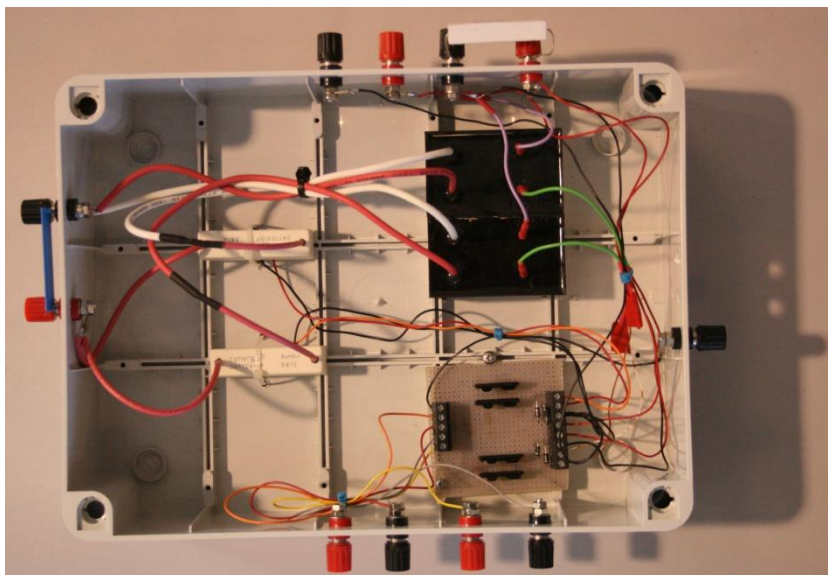


Figure 12: Double EMCO/2 HV switches PCU mock-up realized and tested

A further improvement of the PCU aiming at reducing the device weight might be based on a single EMCO module and four switches. The electric circuit of this improvement is shown in Figure 13.

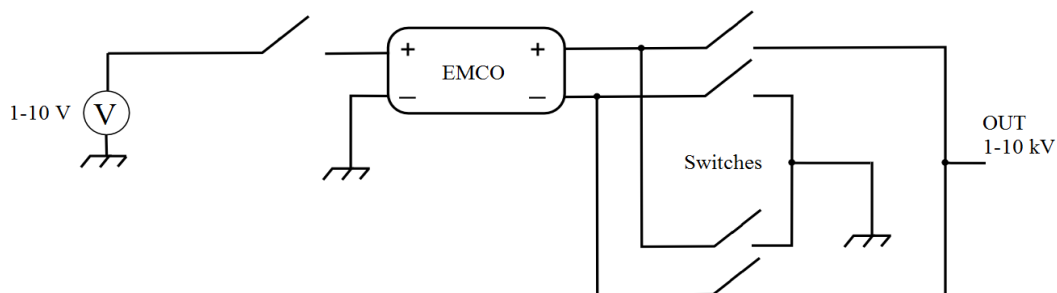


Figure 13: Single EMCO/4 HV switches PCU electric scheme

In both test campaigns the positive or negative voltage was supplied to the emitter and the accelerator was grounded.

### 4.2.3. Beam diagnostic system

The equipment used for the beam diagnostic includes:

- two single filament probes for the beam shape characterization (angle divergence determination),
- a time of flight detector for the beam species characterization.

The beam scan system has been used only during the first test campaign. During the second test campaign the thruster has been run always in high frequency alternate polarity. This did not allow any beam scan since a complete scan requires few minutes to complete. The same holds also for the I-V characteristics that have been recorded only during the first test campaign.

#### 4.2.3.1. Beam scan system

The scanning of the beam was performed with two single filament probes moving inside the beam by means of two stepper motors:

- the vertical probe scanned the beam in the horizontal plane;
- the horizontal probe scanned the beam in the vertical plane.

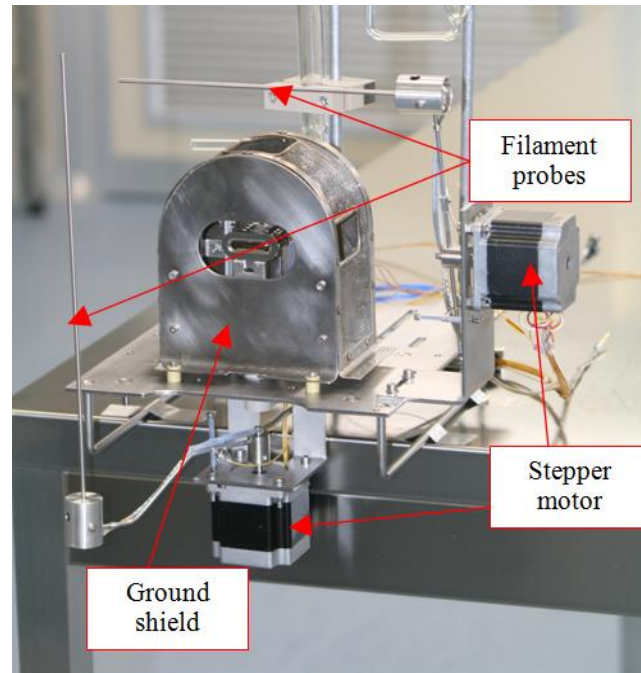


Figure 14: Ionic liquid FEEP setup with diagnostic system

The beam impacting each probe generates a current on the wire that is measured by the detector.

The wire probes are 120 mm in length and 2 mm in diameter.

Both the vertical and the horizontal beam scans are performed by taking 32 measures in the two planes and each measure is computed as the mean of one thousand samples, acquired at a total sample rate of 200 kS/s.

The divergence angles are computed so that they include the 97.5% of the beam current integral.

#### 4.2.3.2. Time of Flight system

Time of Flight measurements aim at assessing the thruster beam composition.

The basic principle behind the ToF method consists in measuring the time required for a charged particle to traverse a certain distance in a region free of external fields. The travel time allows for the computation of the particle's velocity, i.e.

$$v = 2 [(q/m)V_e]^{0.5}$$

where  $V_e$  is the ion source potential and  $(q/m)$  is the specific charge or the charge per unit mass. Known the source potential, the particles velocity formula can be inverted to compute the specific charge.

The simplest way to perform ToF measurements is to suddenly stop the thruster potential and to collect the emitted charged particles by means of a metallic target. The time variation of the collected current gives the travel time of the different beam species and, assuming only single charged ions and particles, their mass.

The expected magnitude of the beam current integral is few microamps and, with a 1 m path, the lowest expected travel time is about  $10^{-5}$  sec.

As a consequence in the experimental setup a suitable switch with a significantly lower response time has been chosen. The switch used for stopping the thruster potential is a fast

high voltage transistor switch (Belhke HTS 201 G/03-GSM), with a turn-on/turn-off rise time lower than 10 ns, see Figure 15.



Figure 15: Fast high voltage switch used for the ToF measurements

In the first test campaign two simple metallic probes are used to collect the current:

- ToF1, a metallic wire placed in vertical position at the centre of the chamber (distance between the emitter tip and the probe: 600 mm),
- ToF2, a metallic target disk placed at the end of the chamber (distance between the emitter tip and the probe: 1300 mm).

In front of the metallic target disk two grids were placed to suppress the secondary electron emission: the first grid was at ground potential, the second one at negative potential (-90 V), see Figure 16.

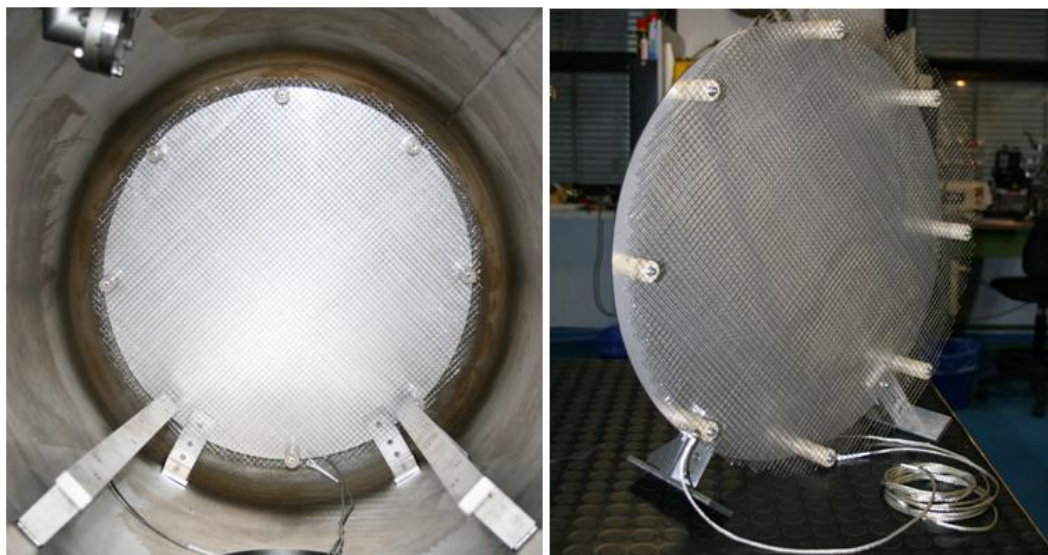


Figure 16: Target mounted in the vacuum chamber (left) and before integration (right)

The beam current collected by the probes is in the range of few microamps and the noise induced from capacitive coupling affects significantly the measurements.

For this reason in the second test campaign an electron multiplier has been used to gain the beam current level. The device is a 18 mm Dual Microchannel Plate (MCP) detectors (Jordan TOF products, Inc), with high gain (about  $10^6$ ) and sub-nanosecond rise time, see Figure 17.



Figure 17: 18mm Dual Microchannel Plate Detector (Jordan TOF Product, Inc)

A micro-channel plate is a slab made from highly resistive material with a regular array of tiny tubes leading from one face to the opposite, densely distributed over the whole surface.

Each microchannel is a continuous-dynode electron multiplier, in which the multiplication takes place under the presence of a strong electric field. The microchannels are parallel to each other. Since the channels are at an angle to the plate, a particle that enters one of the channels hits its wall. The impact starts a cascade of electrons propagating through the channel and the original signal is amplified by several orders of magnitude. Electrons exit the channels on the opposite side and they are detected by a metal anode measuring total current.

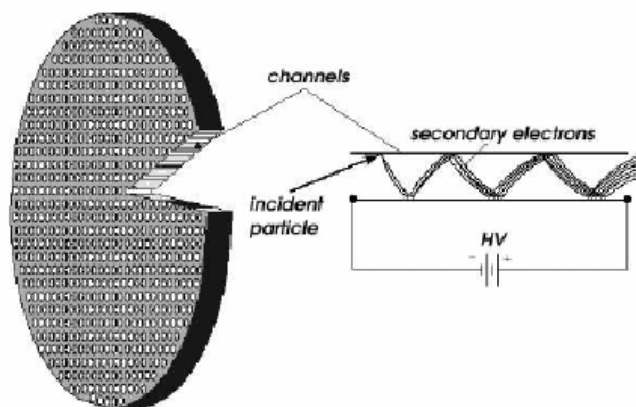


Figure 18: Micro channel plate working principle

The MCP detector, when not used, was covered with a metallic shield to preserve the lifetime of the active surface. The shield also worked as target for emission current detection.

The dual MCP detector was placed at the end of the chamber, see Figure 19, at a distance of 780 mm from the emitter tip.



*Figure 19: Micro channel plate detector.*

In front of the detector a metallic disk was placed for the protection of the detector and was also used to detect the emission of the thruster when the ToF analyses were not performed. The target was polarized by means of a 17 V battery to limit the white noise generated by the power supply.

### **4.3. Preliminary operations**

In both test campaigns the same preliminary operations are required before starting thruster integration and characterization.

### **4.4. Chamber preparation and setup integration**

The chamber is cleaned with water and ethanol, the whole thruster setup and the beam diagnostic system are integrated in the vacuum facility, feed-through connections, and control software are checked.

### **4.5. Propellant outgassing**

Once the chamber pressure decreased below approximately 1 mbar, the liquid propellant in the reservoir started boiling due to the gas dissolved in the bulk volume.

The gas is released at a logarithmic rate, visible bubble formation stops after few hours, but to assure that the whole phenomenon is completed the system has been maintained in this state for at least one day.

### **4.6. Thruster bake out**

The heating of the thruster unit is performed to achieve the appropriate out-gassing of all surfaces, in particular the propellant duct.

The heater power was adjusted to reach 100°C on the emitter unit and the thruster bake out lasted about 170 hours.

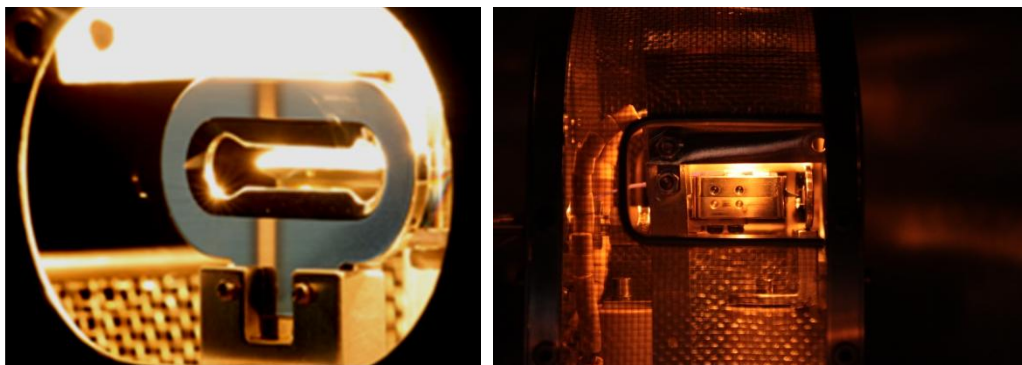


Figure 20: Thruster unit bake-out

#### 4.7. Dry insulation test

Before pouring the propellant and flooding the feeding ducts an electrical test was performed to assure the proper insulation of the electrodes.

The accelerator was grounded and the emitter voltage was increased up to 12 kV and down to -12 kV and the high voltage was maintained for at least 10 minutes.

No leak current or sparks were recorded.

#### 4.8. Propellant pouring

The last operation before starting firing was to pour the liquid propellant into the feeding system.

In the first test campaign an argon pressurizing system was used for pouring the out-gassed liquid from the upper reservoir into the feeding system. In this case after pouring 5 mm of propellant liquid no refurbishing procedures were carried out.

In the second test campaign, a different pouring system was adopted to allow for a fine tuning of the propellant head, thus of the back pressure behind the emitter tip.



Figure 21: Propellant pouring procedure (second test campaign).

## 5. First test campaign results

The first test campaign aimed at giving a preliminary estimation of the main thruster parameters, ie

- onset voltages,
- current-voltage characteristics,
- beam divergence angles,
- beam composition,
- long term behaviour in constant and alternate voltage polarity.

In addition the first set of tests allowed for the identification of a number of experimental problems, i.e. the degradation of the emitter slit, the control of the emitter back pressure and the noise in of ToF measurements, faced with the new setup used for the second test campaign.

In the following the main results about the voltage threshold identification, the current-voltage characteristics, the beam divergence angles and the ToF measurements are summarized.

### 5.1. Onset voltage

After the preliminary operations the emitter voltage was increased to achieve thruster priming and emission.

Theoretical values of emission threshold electrical field for plane and unbounded liquid ion sources can be estimated by the dispersion equation, having  $\text{Re}(s)=0$ ,

$$\rho s^2 = (-Sk^3 + \epsilon_0 E_0^2 - \rho g k) \tanh(kh)$$

where  $g$  is the gravity value,  $\rho$  and  $S$  are the density and the surface tension of liquid,  $\epsilon_0$  the vacuum permittivity,  $k$  the wave number and  $s$  the growth rate.

Critical electric field results to be  $E_c = (2/\epsilon_0 (\rho g S))^{0.5} = 2.3$  kV/mm and, as the actual distance between emitter tip and accelerator is about 2.1 mm, theoretical onset voltage value results to be about 4.9 kV.

This is a very rough approximation useful to determine the lowest theoretical value of the electric field (and of the potential) required for liquid surface instabilization and the experimental value is expected to be larger than this theoretical threshold.

The first emission was detected with the following electrical parameters, see Figure 22:

- $V_e = +8$  kV,
- $V_a = 0$  kV,
- $I_e = 1.2$  uA,
- $I_a = 0$  uA.

Here subscripts indicate emitter (e) and accelerator (a).

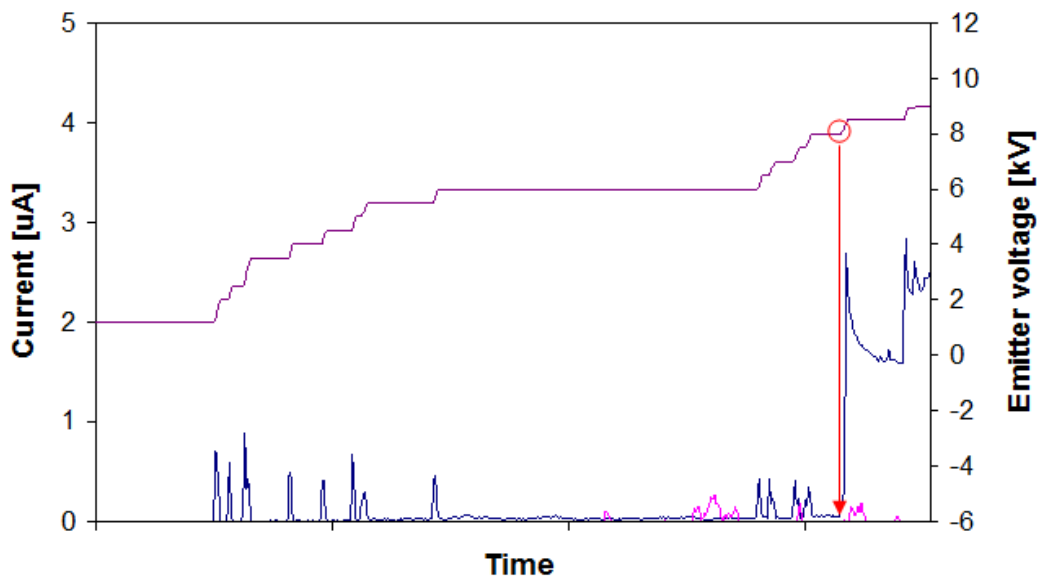


Figure 22: Thruster priming. The onset voltage is indicated by the arrow

Once the thruster was successfully primed, the subsequent activation occurred at relatively lower values.

The emitter current as a function of the emitter voltage close to the thruster activation showed an onset voltage of about 5.5 kV (see Figure 23, where the current was detected by the target, used for shield the ToF detector at the end of the chamber). The experimental value is about 12% larger than the theoretical one.

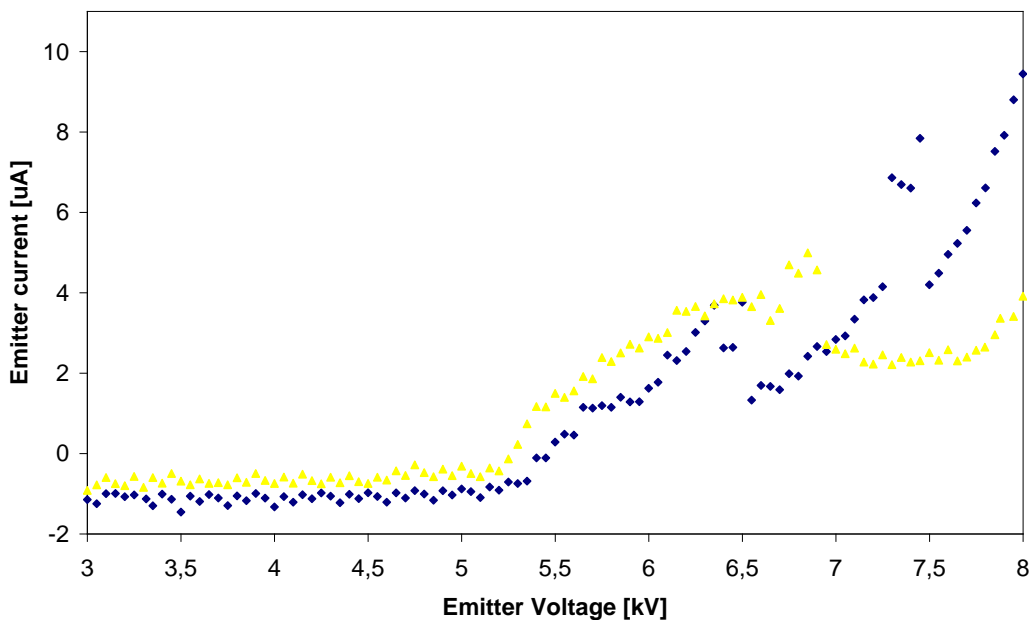


Figure 23: Onset voltage (two different data samples are shown)

The propellant flow rate (as a consequence of backpressure) and the propellant temperature (i.e. the emitter tip temperature) affect the onset voltage.

According to electro spray theory, low propellant rates promote pure ionic regime (PIR)

emission and, as a consequence, low thrust and high specific impulse values. On the contrary high propellant rates produce droplets emission and therefore higher thrust and lower specific impulse values. However, from tests it resulted that a minimum backpressure level seems to be required to have a proper propellant feeding and overcome the high impedance of the emitter channel. Indeed, the emission obtained with too low backpressure values resulted to be unstable, as the emitter current strongly decreased in time with fix applied voltage. 5 mm propellant head used in the first test campaign (i.e. about 0.16 mbar backpressure) was therefore too low for the current emitter configuration. In the second test campaign the refilling system allowed for using different propellant heads.

## 5.2. Current-Voltage characteristics

Current–Voltage (I–V) characteristics were carried out at the end of the test campaign and, since the thruster has been operated for a long time in positive polarity mode (see Sec. 5.5), the data collected might have been affected by operation history. This explains the difference between positive and negative emission, as detailed at the end of Sec. 5.5.

Typical I-V characteristics in positive and negative polarity at 40°C are shown in Figure 24 and Figure 25, respectively.

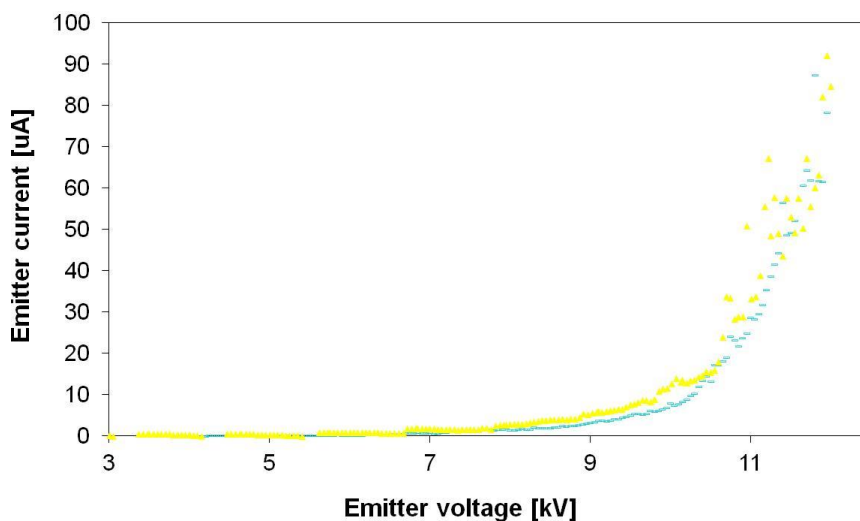


Figure 24: Current-tension characteristic in positive polarity (40°C)

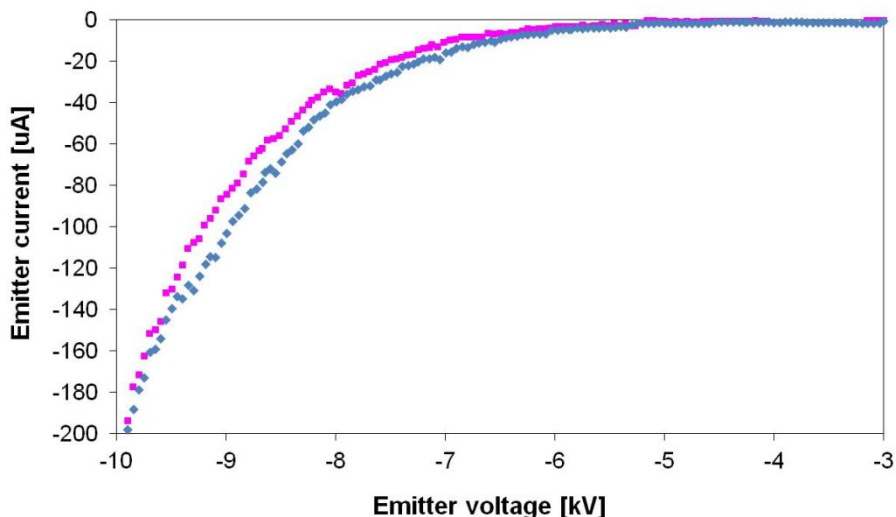


Figure 25: Current-tension characteristic in negative polarity (40°C)

### 5.3. Beam divergence angles

The divergences half angles obtained with the electrostatic probes resulted to be approximately 10 deg in the vertical plane and 30-40 deg in the horizontal plane, see Figure 26 - Figure 35.

The beam divergence half angles resulted to be not very influenced by the emitter temperature, while the currents drained by the probe were highly affected (the probe currents increased of 5 times by varying the emitter temperature from 20°C to 100°C).

The beam scans were carried out successfully only in positive polarity mode. In fact, when the thruster was operated in negative polarity, the secondary electron emission due to the beam impingement on the electrostatic probe produces a net current drained by the probe, which is very low and comparable with the white noise.

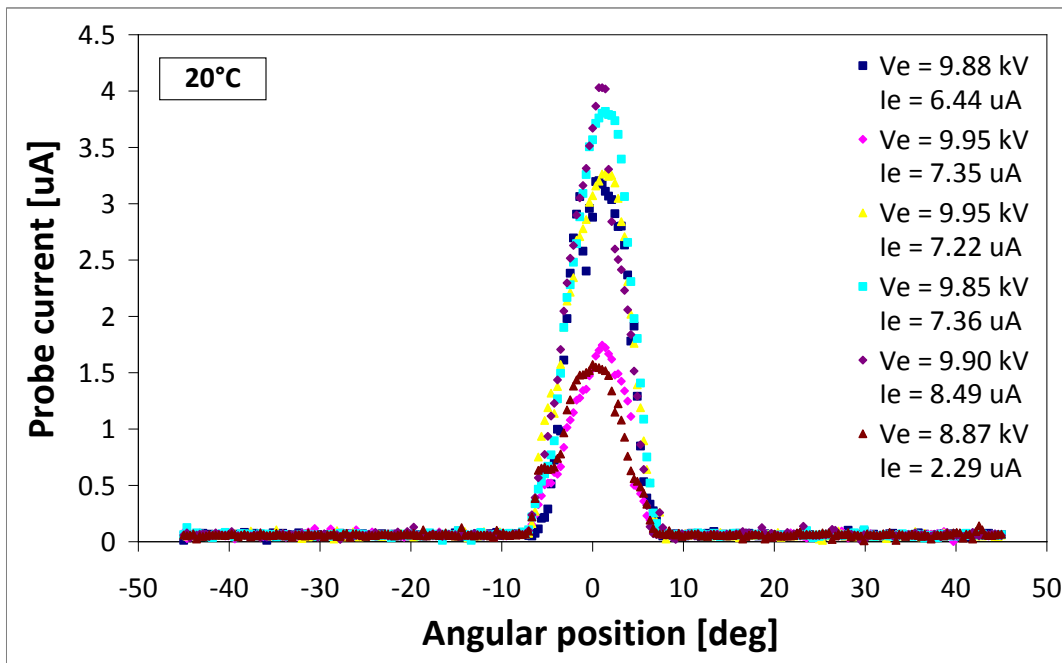


Figure 26: Vertical beam current scans at 20 °C and different emitter voltages

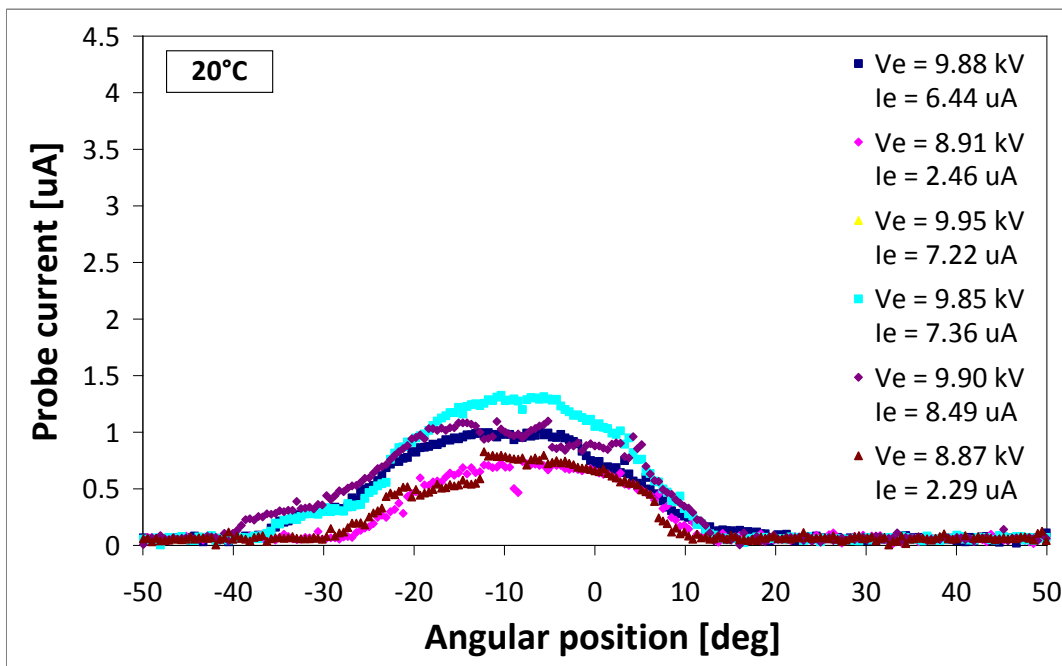


Figure 27: Horizontal beam current scans at 20 °C and different emitter voltages

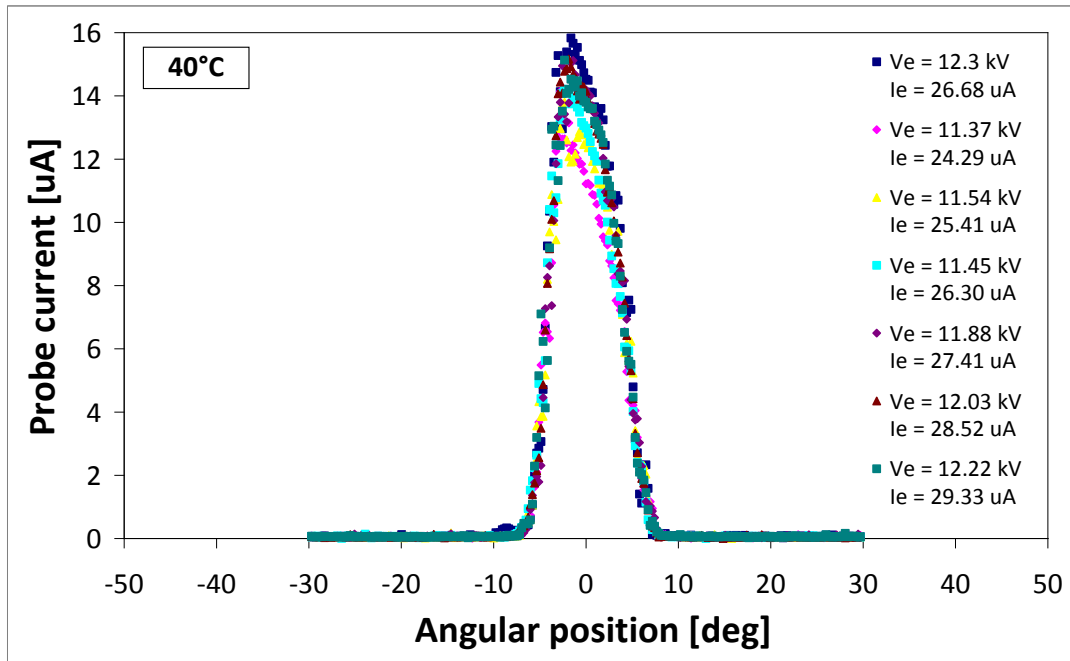


Figure 28: Vertical beam current scans at 40 °C and different emitter voltages

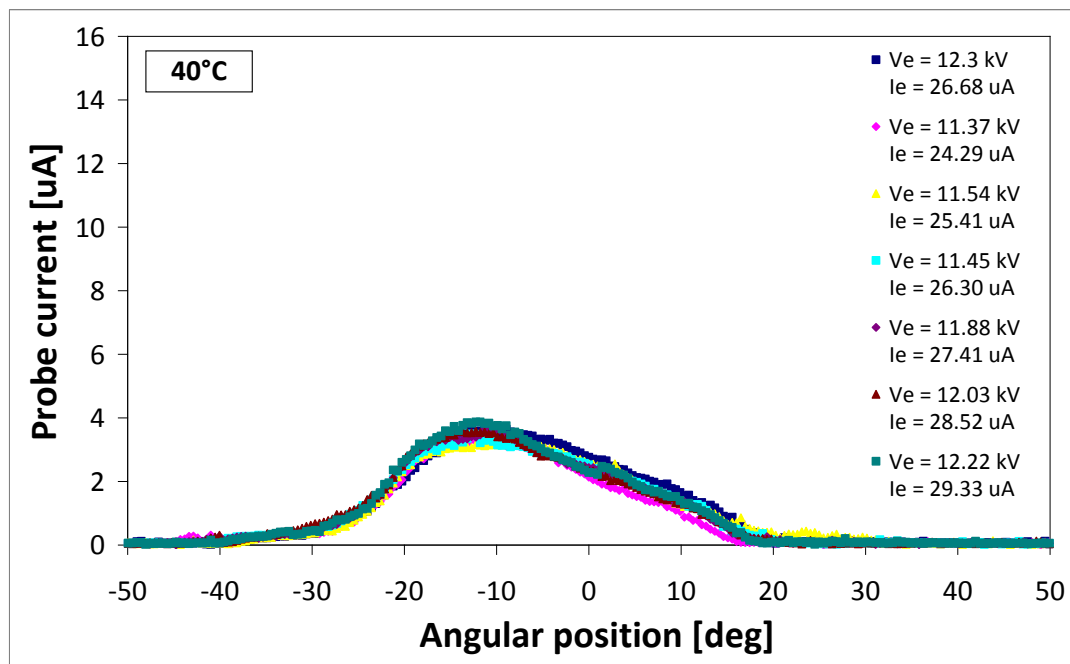


Figure 29: Horizontal beam current scans at 40°C and different emitter voltages

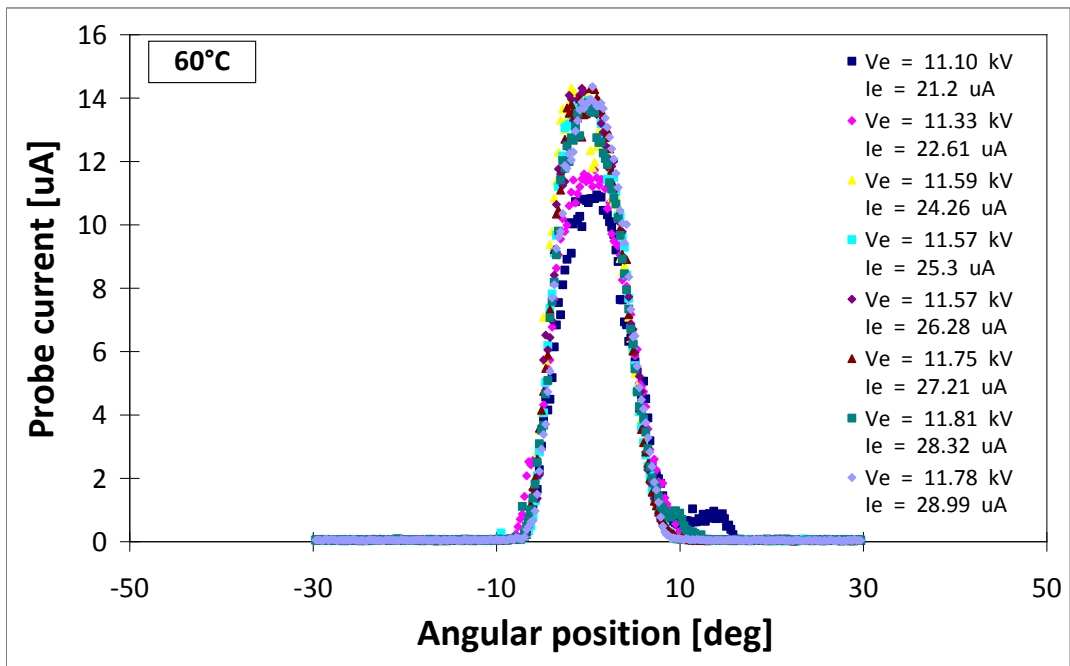


Figure 30: Vertical beam current scans at 60 °C and different emitter voltages

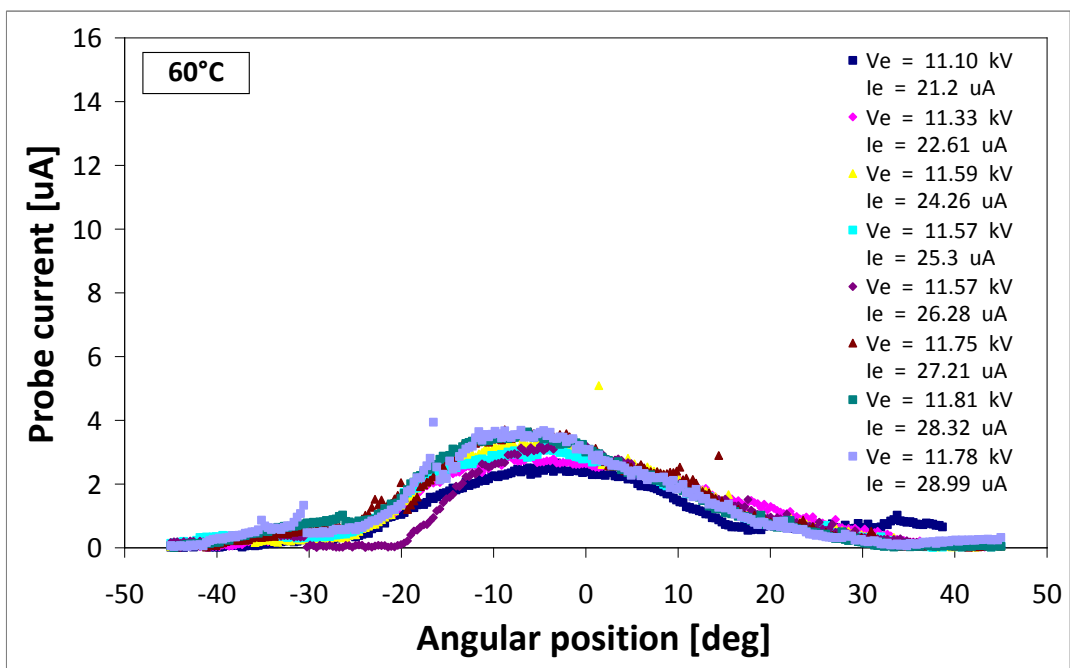


Figure 31: Horizontal beam current scans at 60 °C and different emitter voltages

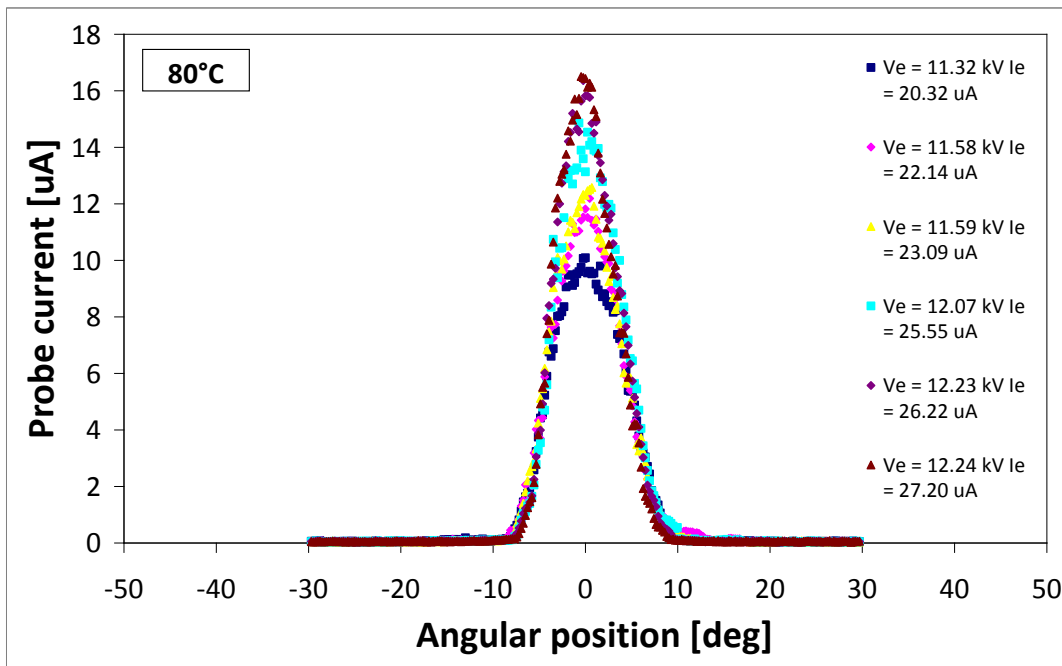


Figure 32: Vertical beam current scans at 80 °C and different emitter voltages

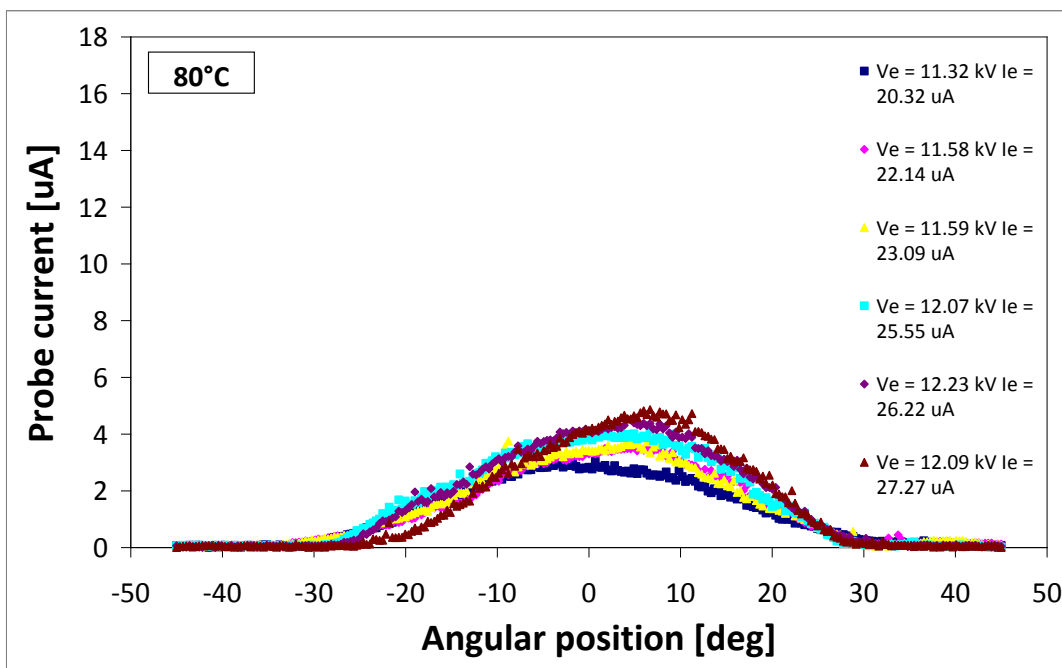


Figure 33: Horizontal beam current scans at 80°C and different emitter voltages

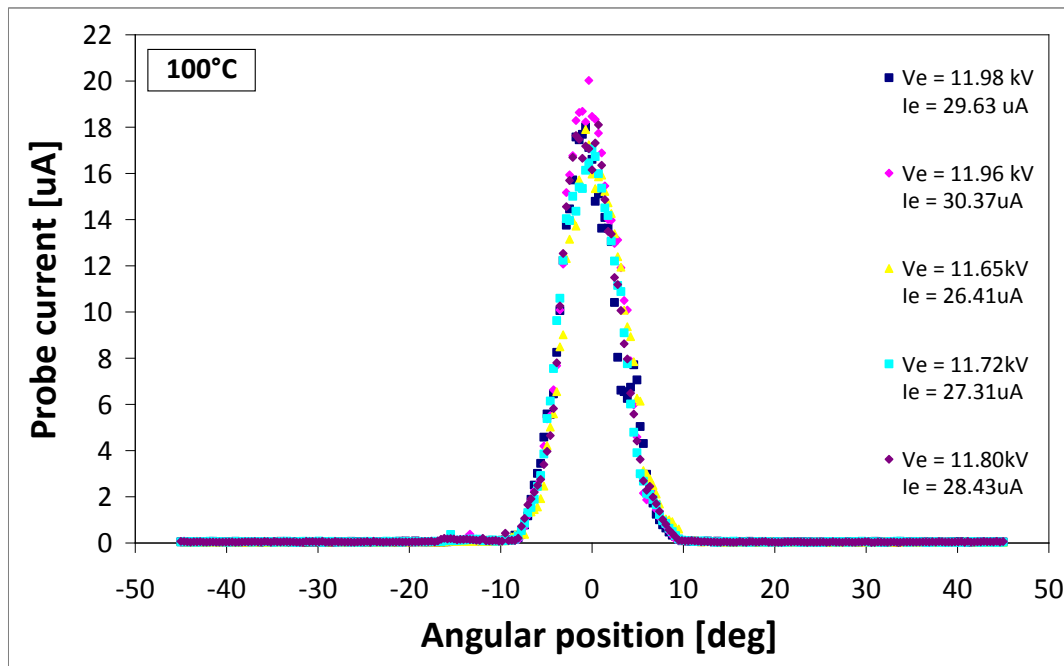


Figure 34: Vertical beam current scans at 100 °C and different emitter voltages

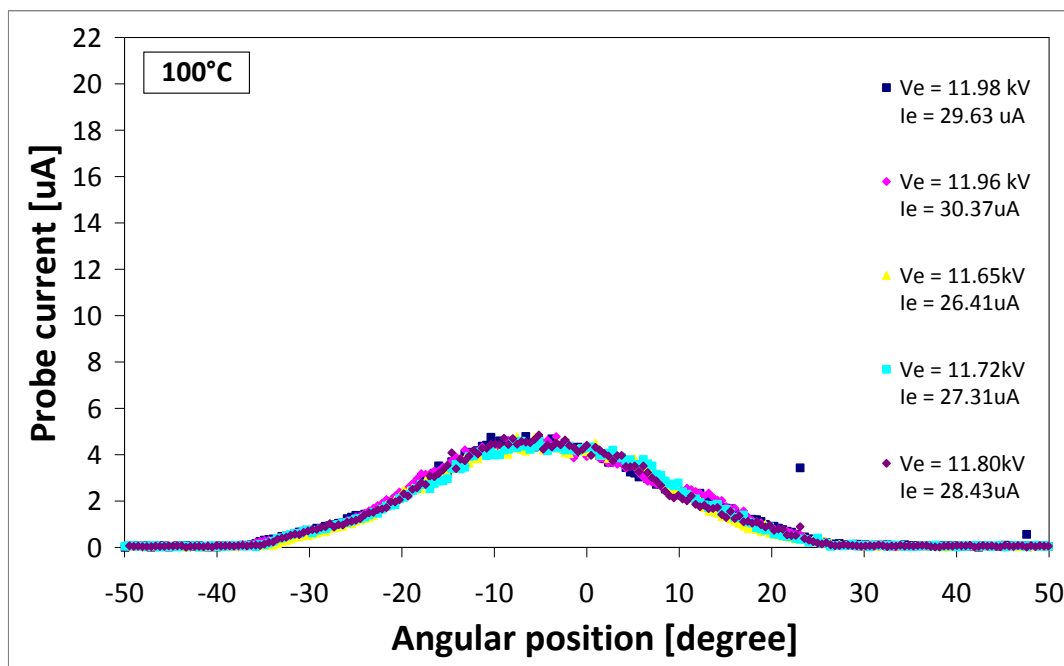


Figure 35: Horizontal beam current scans at 100 °C and different emitter voltages

### 5.4. Time of flight measurements

In the first test campaign, a preliminary solution for the ToF measurement system was adopted (see Sec. 4.2.3.2). The main issue was related to the conditioning of the output signal, because of the very low magnitude of beam current, comparable with the white noise. Also using commercial op-amp (TI’s OPA602 and OPA655) to amplify the signal, a significant dispersion of the data collected remains. In this first set of measurements the

fastest species might have been not detected due to the signal noise. This issue is solved with the setup modified for the second test campaign. Better quality of the data collected was obtained with the thruster operated at high temperature, as the emitted current levels were higher.

The typical outputs of the oscilloscope for the ToF measurements are shown in Figure 38- Figure 39. These measurements are carried out with a temperature of 60, 80, 100 and 120°C, an emitter voltage between 9.2 and 12.9 kV. The time spent by the slowest species to reach the first (ToF1) and second detector (ToF2), see Sec. 4.2.3.2, is identified by the slope variation of voltage curves.

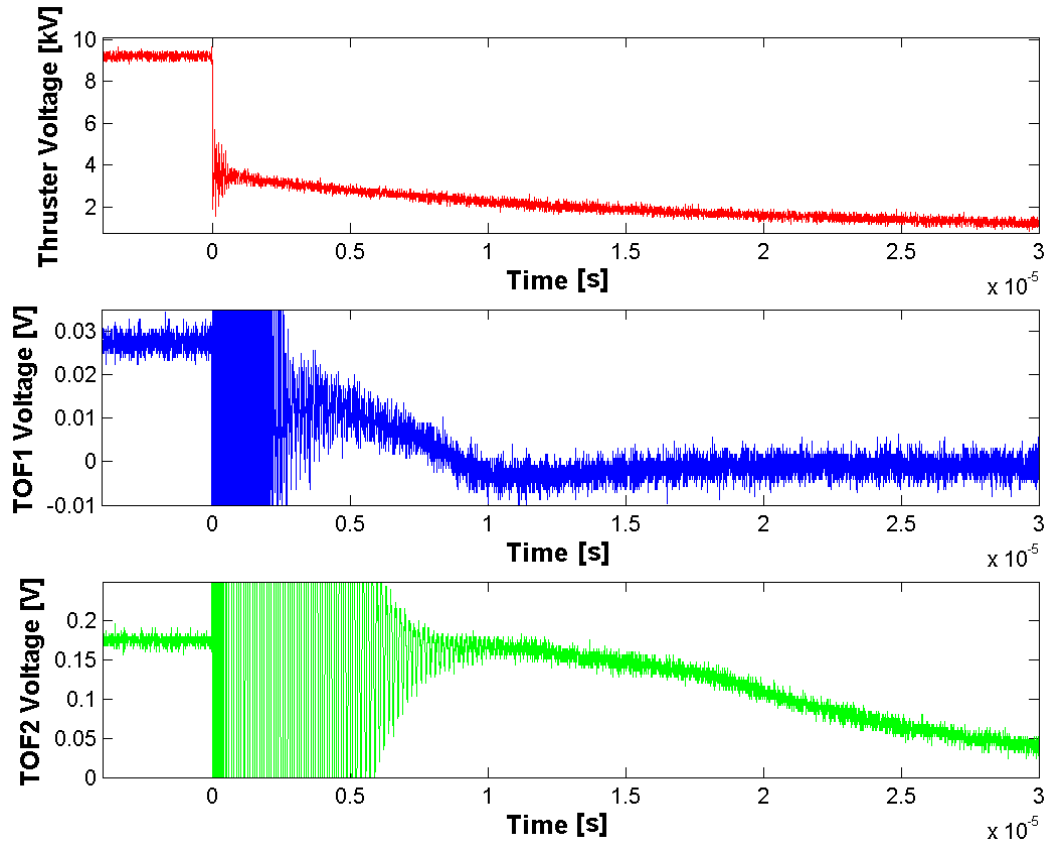


Figure 36: Time-of-Flight measurements. From top to bottom: emitter voltage, ToF1 voltage and ToF2 voltage ( $T_e = 60^\circ\text{C}$ ,  $V_e = 9.2\text{ kV}$ ).

A significant slope variation can be observed

- at  $8.0\ \mu\text{s}$  in the ToF1 voltage graph,
- at  $18.5\ \mu\text{s}$  in the ToF2 voltage graph.

The velocity of the slower species in the beam is

- $v = 0.6\ \text{m} / 8 \cdot 10^{-6}\ \text{s} = 75,000\ \text{m/s}$  (ToF1),
- $v = 1.3\ \text{m} / 18.5 \cdot 10^{-6}\ \text{s} = 70,270\ \text{m/s}$  (ToF2).

The corresponding mass to charge ratio is

- $m/q = 2 V_e / v^2 = 2 \cdot 9.2 \cdot 10^3\ \text{V} / (75,000\ \text{m/s})^2 = 3.27 \cdot 10^{-6}\ \text{kg/C}$  (ToF1),
- $m/q = 2 V_e / v^2 = 2 \cdot 9.2 \cdot 10^3\ \text{V} / (70,270\ \text{m/s})^2 = 3.73 \cdot 10^{-6}\ \text{kg/C}$  (ToF2).

Assuming only single charge species, the molecular mass is

- $M = 3.27 \cdot 10^{-6}\ \text{kg/C} \cdot 1.6 \cdot 10^{-19}\ \text{C} / 1.66 \cdot 10^{-27}\ \text{kg} = 313.2$  (ToF1),
- $M = 3.73 \cdot 10^{-6}\ \text{kg/C} \cdot 1.6 \cdot 10^{-19}\ \text{C} / 1.66 \cdot 10^{-27}\ \text{kg} = 357.3$  (ToF2).

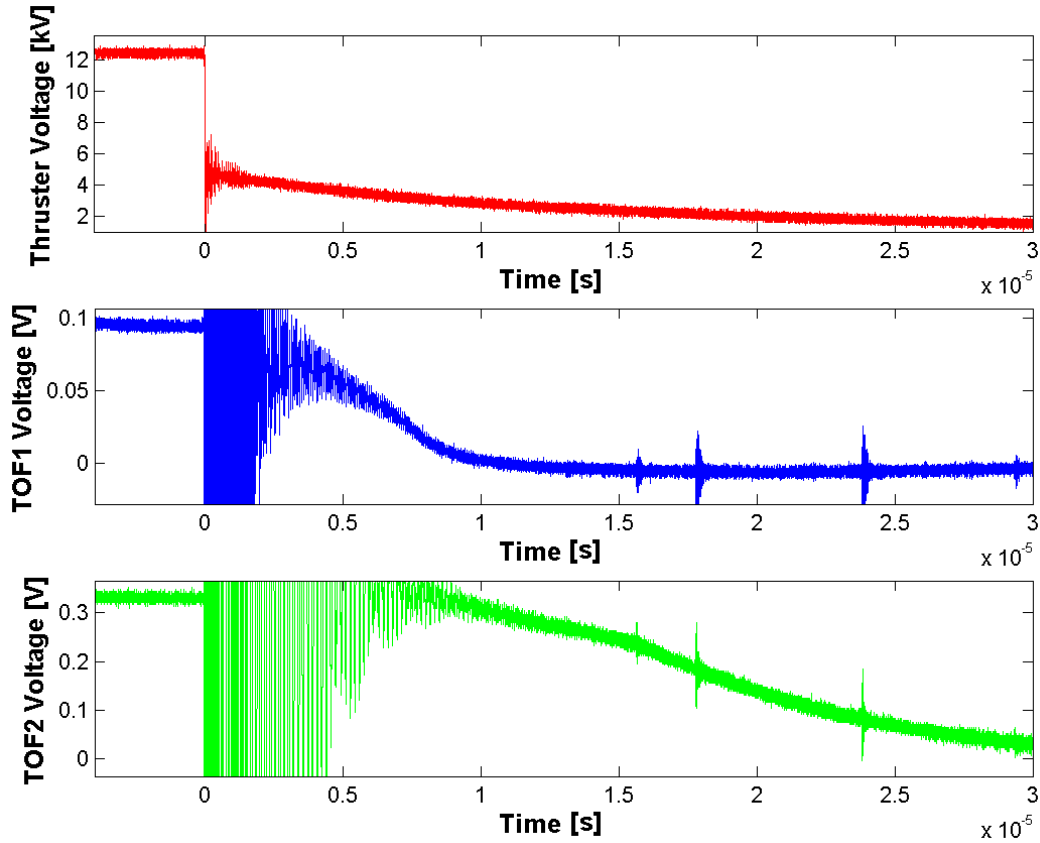


Figure 37: Time-of-Flight measurements. From top to bottom: emitter voltage, ToF1 voltage and ToF2 voltage ( $T_e = 80^\circ\text{C}$ ,  $V_e = 12.5\text{ kV}$ ).

A significant slope variation can be observed

- at  $6.9\ \mu\text{s}$  in the ToF1 voltage graph,
- at  $15.7\ \mu\text{s}$  in the ToF2 voltage graph.

The velocity of the slower species in the beam is

- $v = 0.6\ \text{m} / 6.9 \cdot 10^{-6}\ \text{s} = 86,956\ \text{m/s}$  (ToF1),
- $v = 1.3\ \text{m} / 15.7 \cdot 10^{-6}\ \text{s} = 82,802\ \text{m/s}$  (ToF2).

The corresponding mass-to-charge ratio is

- $m/q = 2 V_e / v^2 = 2 \cdot 12.5 \cdot 10^3\ \text{V} / (86,956\ \text{m/s})^2 = 3.33 \cdot 10^{-6}\ \text{kg/C}$  (ToF1),
- $m/q = 2 V_e / v^2 = 2 \cdot 12.5 \cdot 10^3\ \text{V} / (82,802\ \text{m/s})^2 = 3.64 \cdot 10^{-6}\ \text{kg/C}$  (ToF2).

Assuming only single charge species, the molecular mass is

- $M = 3.33 \cdot 10^{-6}\ \text{kg/C} \cdot 1.6 \cdot 10^{-19}\ \text{C} / 1.66 \cdot 10^{-27}\ \text{kg} = 319.0$  (ToF1),
- $M = 3.64 \cdot 10^{-6}\ \text{kg/C} \cdot 1.6 \cdot 10^{-19}\ \text{C} / 1.66 \cdot 10^{-27}\ \text{kg} = 348.7$  (ToF2).

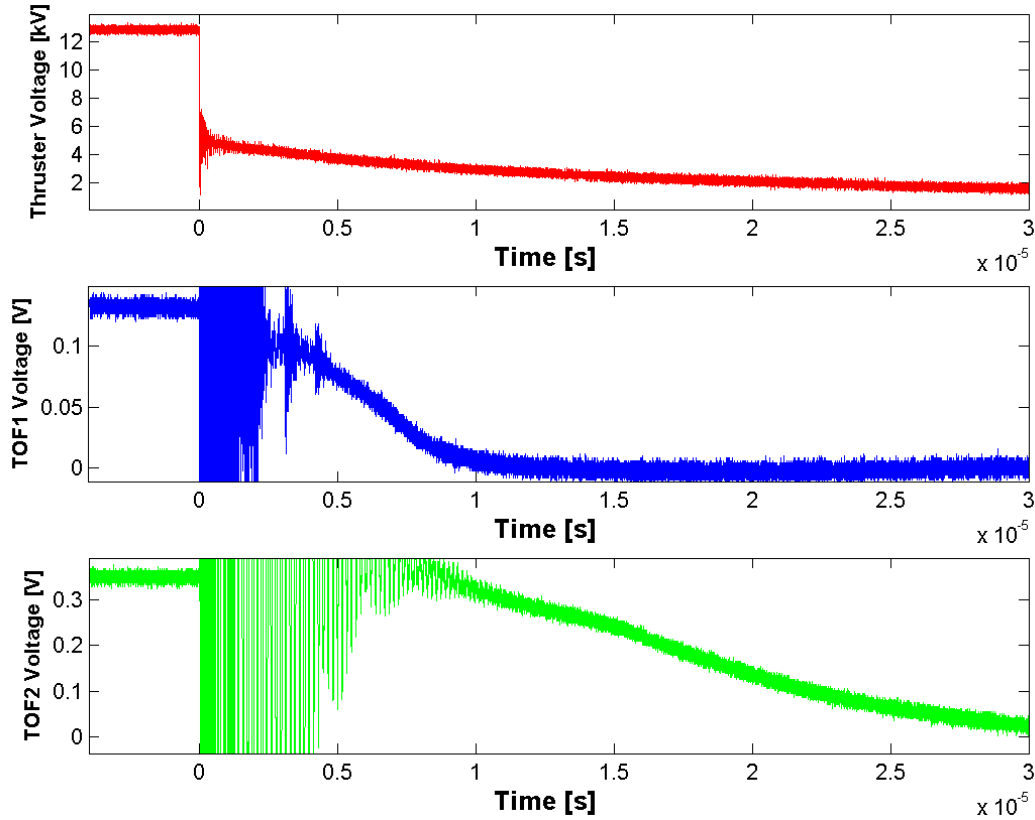


Figure 38: Time-of-Flight measurements. From top to bottom: emitter voltage, ToF1 voltage and ToF2 voltage ( $T_e = 100^\circ\text{C}$ ,  $V_e = 12.9$  kV).

A significant slope variation can be observed

- at  $6.8 \mu\text{s}$  in the ToF1 voltage graph,
- at  $15.4 \mu\text{s}$  in the ToF2 voltage graph.

The velocity of the slowest species in the beam is

- $v = 0.6 \text{ m} / 6.8 \cdot 10^{-6} \text{ s} = 88235 \text{ m/s}$  (ToF1),
- $v = 1.3 \text{ m} / 15.4 \cdot 10^{-6} \text{ s} = 84416 \text{ m/s}$  (ToF2).

The mass-to-charge ratio is

- $m/q = 2 V_e / v^2 = 2 \cdot 12.9 \cdot 10^3 \text{ V} / (88235 \text{ m/s})^2 = 3.31 \cdot 10^{-6} \text{ kg/C}$  (ToF1),
- $m/q = 2 V_e / v^2 = 2 \cdot 12.9 \cdot 10^3 \text{ V} / (84416 \text{ m/s})^2 = 3.62 \cdot 10^{-6} \text{ kg/C}$  (ToF2).

Assuming only single charge species, the molecular mass is

- $M = 3.31 \cdot 10^{-6} \text{ kg/C} \cdot 1.6 \cdot 10^{-19} \text{ C} / 1.66 \cdot 10^{-27} \text{ kg} = 317.4$  (ToF1),
- $M = 3.59 \cdot 10^{-6} \text{ kg/C} \cdot 1.6 \cdot 10^{-19} \text{ C} / 1.66 \cdot 10^{-27} \text{ kg} = 346.8$  (ToF2).

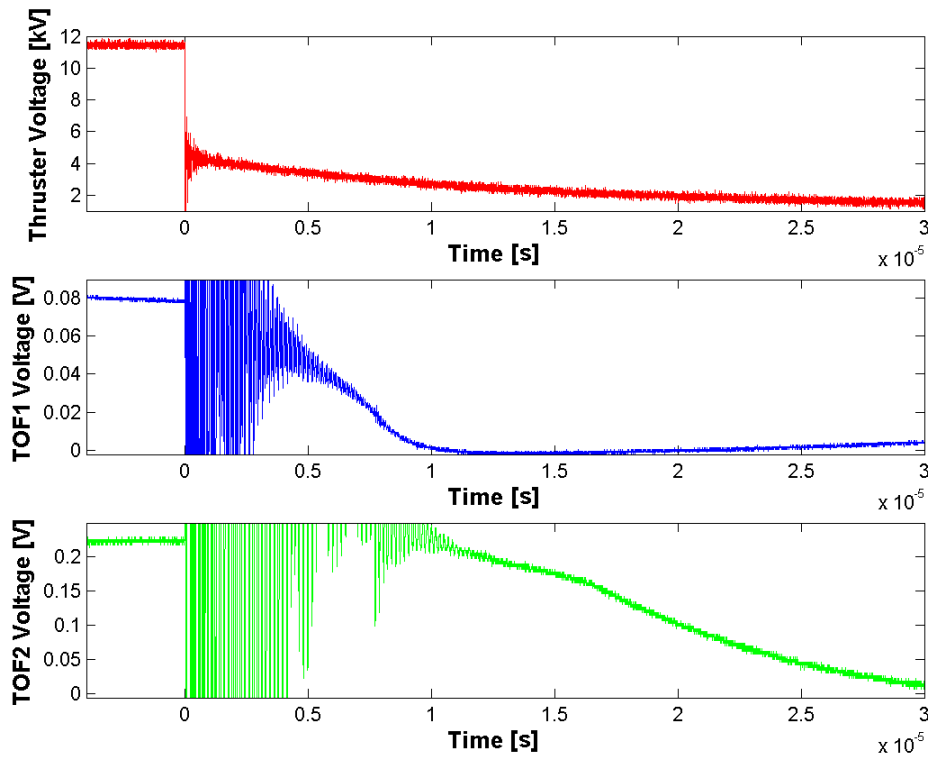


Figure 39: Time-of-Flight measurements. From top to bottom: emitter voltage, ToF1 voltage and ToF2 voltage ( $T_e = 120^\circ\text{C}$ ,  $V_e = 11.5\text{ kV}$ ).

A significant slope variation can be observed

- at  $7.5\ \mu\text{s}$  in the ToF1 voltage graph,
- at  $16.6\ \mu\text{s}$  in the ToF2 voltage graph.

The velocity of the slower species in the beam was

- $v = 0.6 / 7.5 \cdot 10^{-6}\ \text{m/s} = 80,000\ \text{m/s}$  (ToF1),
- $v = 1.3 / 16.6 \cdot 10^{-6}\ \text{m/s} = 78,313 \cdot 10^3\ \text{m/s}$  (ToF2).

The corresponding mass-to-charge ratio is

- $m/q = 2 V_e / v^2 = 2 \cdot 11.5 \cdot 10^3\ \text{V} / (80,000\ \text{m/s})^2 = 3.59 \cdot 10^{-6}\ \text{kg/C}$  (ToF1),
- $m/q = 2 V_e / v^2 = 2 \cdot 11.5 \cdot 10^3\ \text{V} / (78,313\ \text{m/s})^2 = 3.75 \cdot 10^{-6}\ \text{kg/C}$  (ToF2).

Assuming only single charge species, the molecular mass is

- $M = 3.59 \cdot 10^{-6}\ \text{kg/C} \cdot 1.6 \cdot 10^{-19}\ \text{C} / 1.66 \cdot 10^{-27}\ \text{kg} = 344.2$  (ToF1),
- $M = 3.75 \cdot 10^{-6}\ \text{kg/C} \cdot 1.6 \cdot 10^{-19}\ \text{C} / 1.66 \cdot 10^{-27}\ \text{kg} = 359.2$  (ToF2).

Table 1 summarizes the ToF measurements for the complete range of operating conditions investigated.

Measurement carried out at  $20$  and  $40^\circ\text{C}$  are not presented, as the beam current collected on the target resulted very low, comparable with the white noise.

Temperature [°C]	Applied voltage [kV]	Distance [m]	ToF [us]	Velocity [m/s]	m/q [kg/C]	Molecular mass [amu]
60°C	9.2	0.6	8.0	75,000	$3.27 \cdot 10^{-6}$	313.2
		1.3	18.5	70,270	$3.73 \cdot 10^{-6}$	357.3
80°C	12.4	0.6	6.9	86,956	$3.33 \cdot 10^{-6}$	319.0
		1.3	15.7	82,802	$3.64 \cdot 10^{-6}$	348.7
100°C	12.9	0.6	6.8	88,235	$3.31 \cdot 10^{-6}$	317.4
		1.3	15.4	84,416	$3.62 \cdot 10^{-6}$	346.8
120°C	11.5	0.6	7.5	80,000	$3.59 \cdot 10^{-6}$	344.2
		1.3	16.6	78,313	$3.75 \cdot 10^{-6}$	359.2

Table 1: Time-of-Flight data summary for 9–13 kV emitter voltage and 60–100 °C operating temperature

The small differences between the values obtained from the two probes can be explained by the large differences in probe geometry: the wire probe (ToF1) achieves a local measurement on a restricted portion of the beam, while the target (ToF2) collects the current over a very large beam portion.

Ionic compounds that are favourite candidates to be present in the beam are  $\text{EMI}^+$  (monomers),  $(\text{EMI-BF}_4)\text{EMI}^+$  (dimers) and  $(\text{EMI-BF}_4)_2\text{EMI}^+$  (trimers). The molecular masses of these compounds are summarized in table 2.

Ionic compound	Molecular mass [amu]
$\text{EMI}^+$	111.165
$(\text{EMI-BF}_4)\text{EMI}^+$	309.135
$(\text{EMI-BF}_4)_2\text{EMI}^+$	507.105

Table 2: Molecular masses of  $\text{EMI-BF}_4$  ionic compounds

The dimer molecular mass of  $\text{EMI-BF}_4$  is close to the values of the slowest species detected by means of ToF measurements. Accordingly the thruster beam likely contains a limited number of heavier ion clusters or droplets.

These data are refined with the results of ToF measurements of the second test campaign.

## 5.5. Endurance test

The thruster prototype was operated in constant positive polarity mode, constant negative polarity mode and alternate polarity mode.

The total firing time was 532 hours (see Figure 40); the thruster fired

- in positive polarity mode for 210 hours,
- in negative polarity mode for 36 hours in negative polarity,
- in alternate polarity mode for 284 hours, with a switch frequency of 1/60 and 1/120 Hz (see Figure 41).

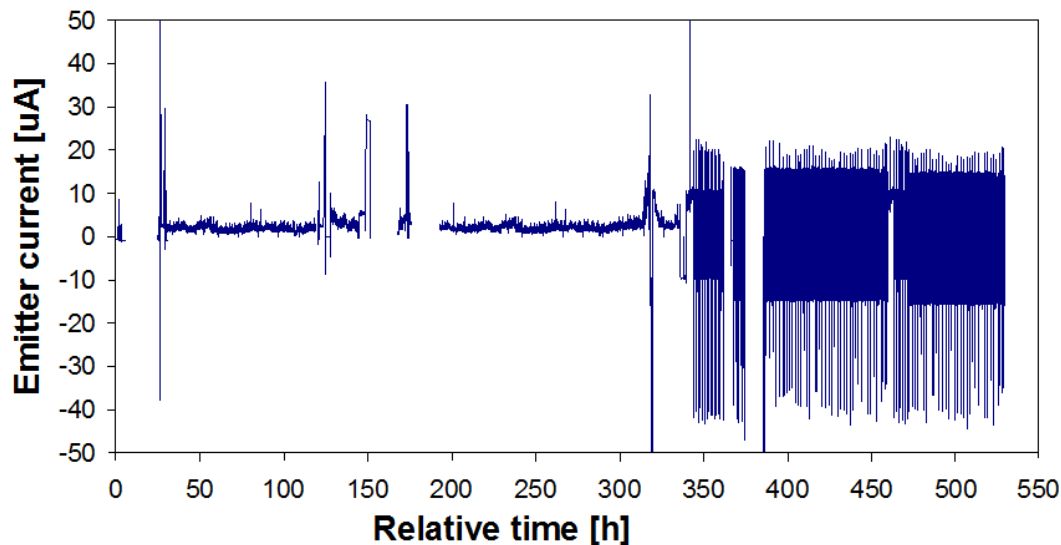


Figure 40: Emitter current trend over the whole thruster testing

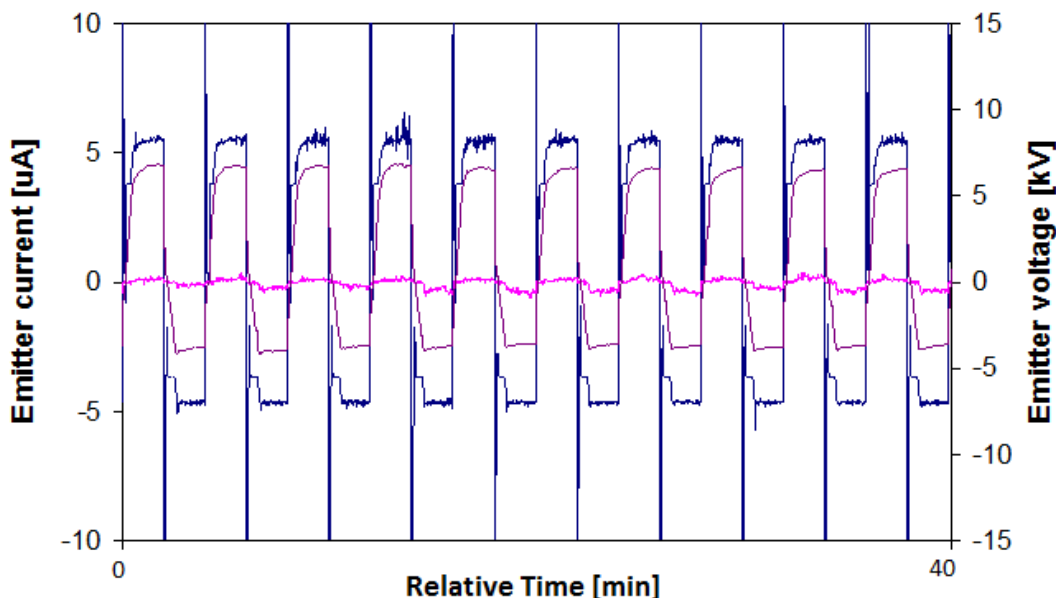


Figure 41: Emitter current, accelerator current and emitter voltage trend in alternate polarity (20 cycles)

As shown in Figure 40, the thruster has been operated for the first phase of the test campaign in continuous polarity mode, while the alternate polarity has been tested after about 250 hours of firing.

It is reasonable to assume that the thrust history might have affected the overall thruster behaviour.

During the emission non-ejected ions grow into the liquid bulk and, given a sufficiently long time, they are attracted toward the emitter boundaries where they electrochemically react with the emitter material. In the EMI-BF<sub>4</sub> case, positive species react producing a surface degradation, while negative ones releasing gas. In both cases the propellant exhausted but not ejected tends to accumulate debris along the emitter tip.

These phenomena may be overcome by means of a suitable alternation between positive and negative polarity, so that the potential difference across the double layer formed between the emitter conductive surface and the liquid is maintained below the electrochemical window limit of the EMI-BF<sub>4</sub>. The critical time to raise the double-layer potential above the electrochemical window of the liquid is given by:

$$t_w^\pm = \epsilon\epsilon_0 \frac{V_w^\pm A_e}{I\delta_{dl}}$$

where  $I$  is the current,  $\epsilon_0$  is the dielectric constant of vacuum,  $\epsilon$  and  $V_w^\pm$  the dielectric constant and the electrochemical window limit of EMI-BF<sub>4</sub>,  $\delta_{dl}$  the double layer thickness and  $A_e$  the emitter surface in contact with the liquid.

For EMI-BF<sub>4</sub> the thickness of the double layer, close to the anion/cation diameter, can be assumed to be equal to  $\delta_{dl} \approx 5 \times 10^{-10}$  m, the dielectric constant is  $\epsilon \approx 70$ , the electrochemical window is  $V_w^\pm \approx 4.3$  V. The emitter wetted area is about 50 mm<sup>2</sup>, but the active area interested by the phenomena is probably much smaller. For currents ranging from 10 to 100  $\mu$ A the time before electrochemical reactions set varies in the range 1-10 sec.

In the first test campaign the power supply used didn't allow for a switching frequency high enough. As a consequence the thruster was not operated in optimal conditions and some liquid degradation occurred during the tests and a significant asymmetry was detected between positive and negative characteristics. In the second test campaign, see Sec. 6, the thruster has been always run in alternate polarity mode.

## 6. Second test campaign results

The second test campaign aimed at giving a refined estimation of the main thruster parameters, i.e.

- behaviour in alternate voltage polarity mode,
- onset voltages,
- beam composition.

and to test the PCU breadboard, see Sec. 4.2.2, for thruster operation. Instead current-voltage characteristics and beam divergence angles were not further investigated, since the thruster was always operated in alternate polarity mode (see Sec. 6.1 for details).

In addition the first set of test allowed for the identification of a number of experimental problems, i.e. the degradation of the emitter slit, the control of the emitter back pressure and the noise in ToF measurements, faced with the setup used for the second test campaign.

In the following the main results about the voltage threshold identification, the beam divergence angles and the ToF measurements are summarized.

As in the previous test campaign, initially the test was started with 5 mm of propellant head. The emission obtained with the corresponding backpressure value resulted to be again unstable, as the emitter current decreased in time also with a fixed voltage applied, see Figure 42.

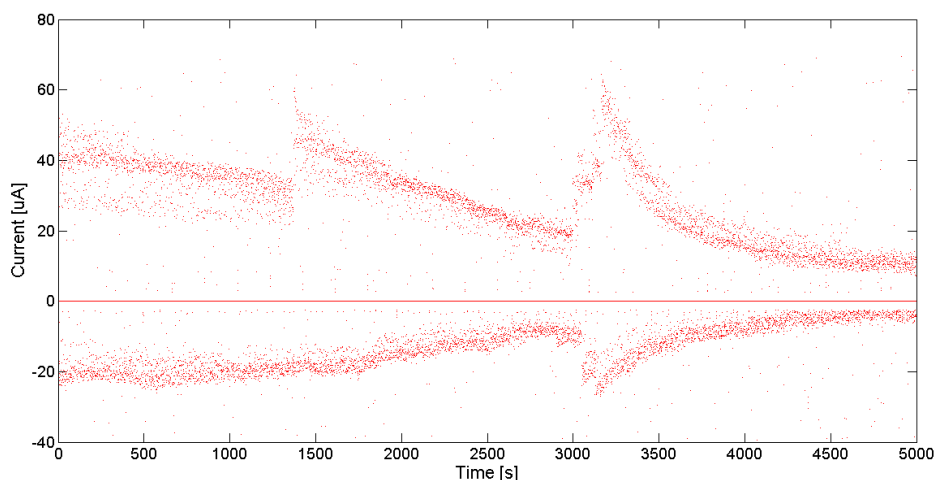


*Figure 42: Emitter current evolution in time with a 5 mm propellant head*

Further propellant was then poured in the feeding system to obtain a more stable emission, see Figure 43 - Figure 46.

The final propellant head was about 31 mm, corresponding to 3.7 mbar backpressure.

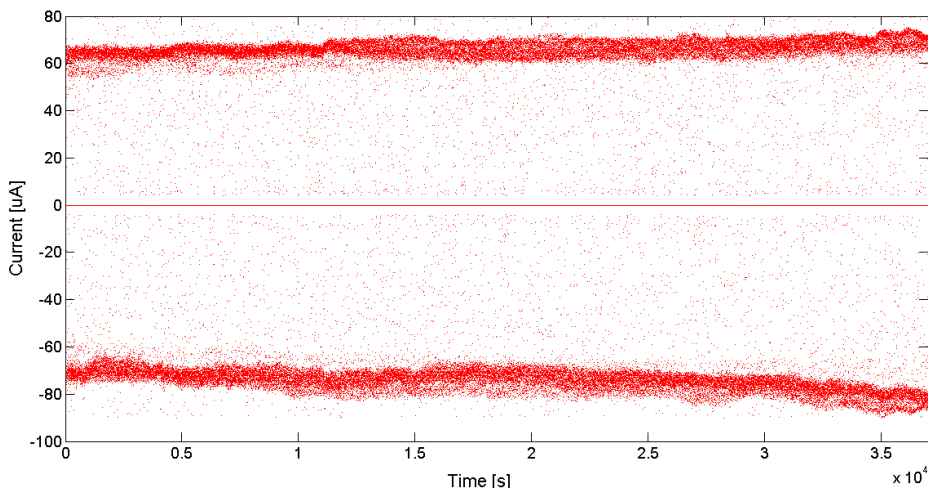


Figure 43: Emitter current (pos voltage=+7.5 kV, neg voltage=-7.6 kV, emitter temperature=110°C, high-state time=50 ms)

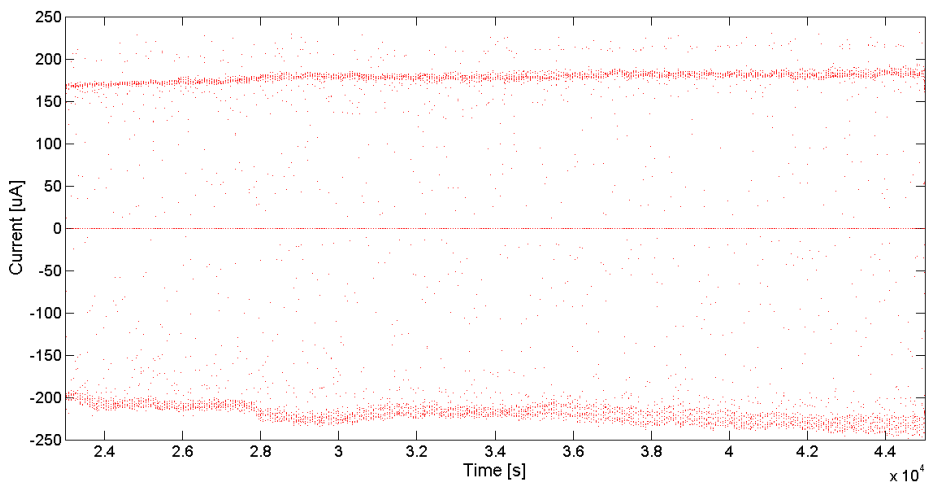


Figure 44: Emitter current (pos voltage=+8.2 kV, neg voltage=-8.4 kV, emitter temperature=110°C, high-state time=50 ms)

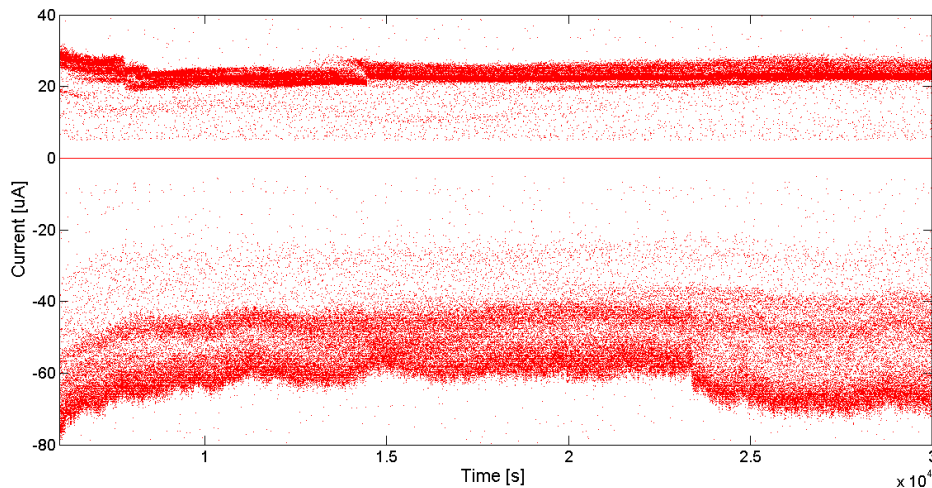


Figure 45: Emitter current (pos voltage=+6.7 kV, neg voltage=-6.94 kV, emitter temperature=70°C, high-state time=200 ms)

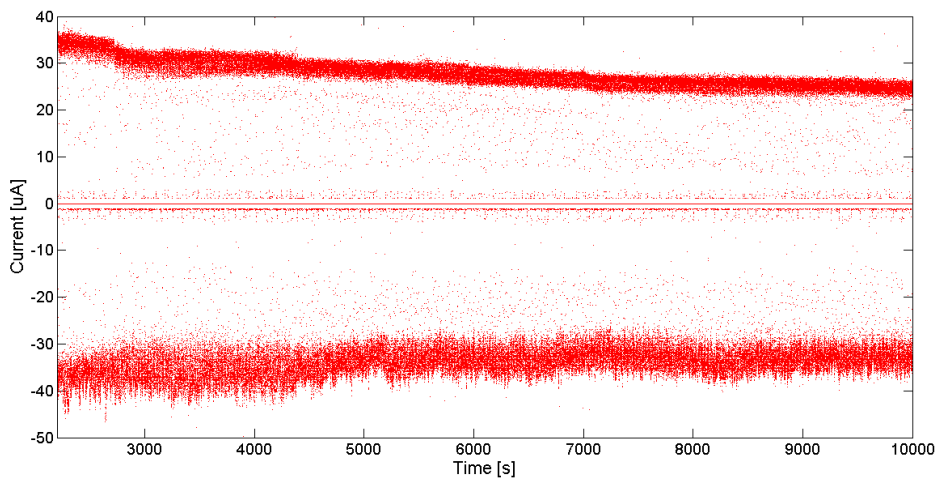


Figure 46: Emitter current (pos voltage=+6.9 kV, neg voltage=-7.0 kV, emitter temperature=83°C, high-state time=1000 ms)

### 6.1. Alternate voltage polarity mode

The thruster was always operated in alternate polarity mode, besides when ToF measurements were carried out.

Figure 47 shows the typical cycle implemented:  $\tau$  is the high-state time (positive or negative voltage) and  $t$  is the total cycle time ( $t/2$  is the switching frequency).

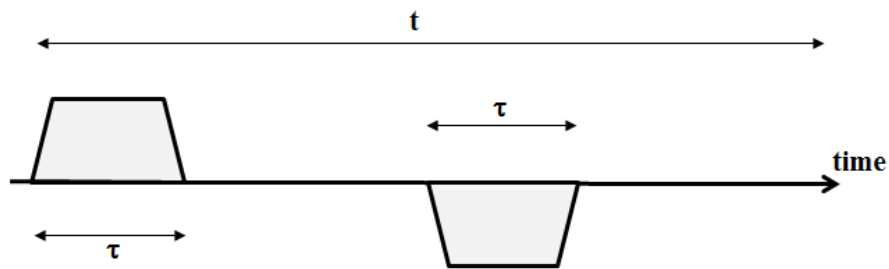


Figure 47: Alternate polarity cycle sketch

A low-state time longer than zero is used to preserve the lifetime of the reed relays. In this way the switches always commute the on/off states when the voltage is not applied to the emitter. This allows for avoiding arch discharging between the relay contacts.

During the test the values of  $\tau$  ranged from 50 ms to 4000 ms and the corresponding duty cycles from 4% to 76%.

In Sec. 5.5 minimum  $\tau$  values required for avoiding electrochemical reactions between propellant and emitter are estimated to be in the range 1-10 s, depending on the emission current. Shorter  $\tau$  values have been used both to take some security margins and to test the capability of the thruster to cope with the charging RU issue.

The polarity switching did not pointed out specific thruster operation problems, even at high frequency. However with applied voltages close to the onset value, too short  $\tau$  values did not allow for the simultaneous activation of all emission sites along the slit. In this case the emission current resulted to be stepwise in time, see Figure 48.

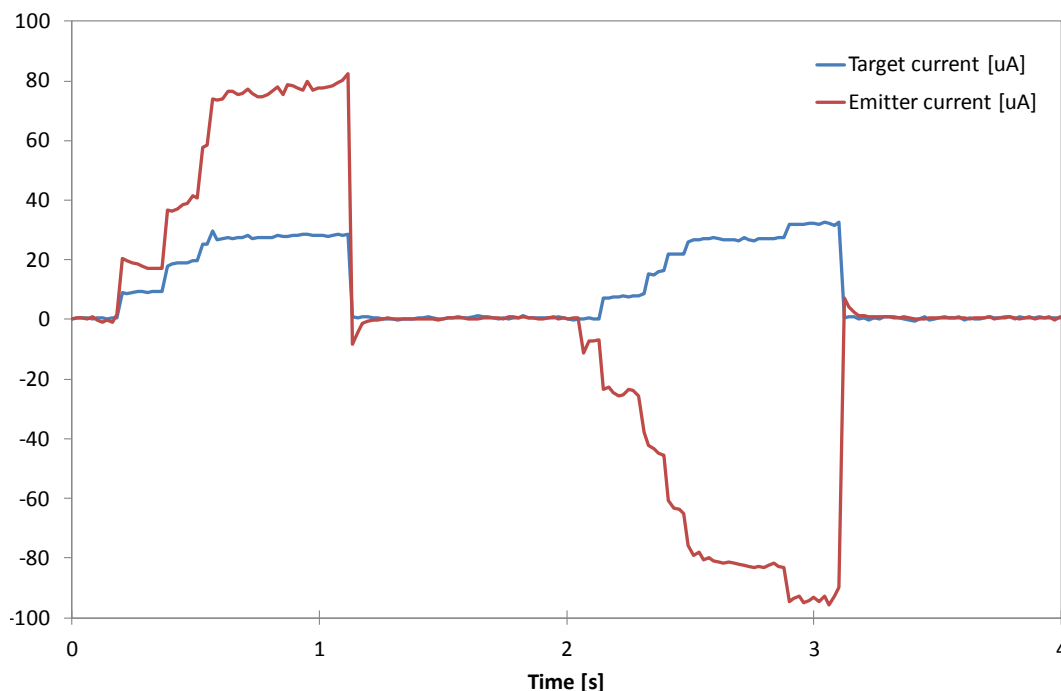


Figure 48: Current stepwise trend ( $V = \pm 6 \text{ kV}$ )

The thruster worked for a total of 467 hours always in alternate polarity with an active firing time of 213 hours. Table 3 summarizes the cycle characteristics and the total firing time accumulated during the test campaign.

Cycle time [ms]	Cycle number	$\tau$ [ms]	Working time [h]	POS firing time [h]	NEG firing time [h]	Firing time [h]
2200	219571	50 200	134.2	6.7	6.7	13.3
3800	54383	1000	57.5	15.0	14.9	30.0
10400	733	4000	2.1	0.8	0.8	1.6
12000	14939	4000	49.8	16.6	16.6	33.2
12800	140800	4000	213.1	66.6	66.6	133.2
16000	1437	1000 1500 4000	6.4	0.8	0.9	1.7
16900	842	1000	4.0	0.1	0.2	0.3
<b>Total</b>			<b>467.0</b>	<b>106.6</b>	<b>106.7</b>	<b>213.3</b>

Table 3: Alternate polarity cycles and firing time summary

## 6.2. Onset Voltage

The activation after the refuelling (31 mm propellant head) occurred at lower values than the first test campaign.

As an example Figure 49 shows an onset voltage of about 5.7 kV in positive polarity and -5.1 kV in negative polarity (27°C).

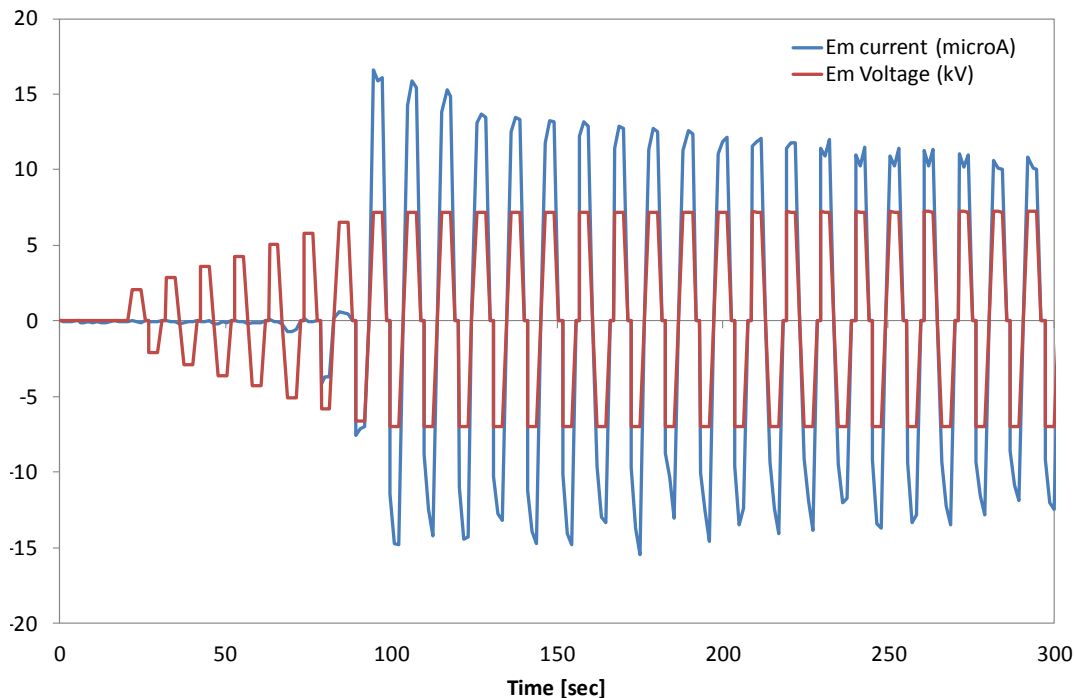


Figure 49: Onset voltage

### 6.3. Beam divergence angles

During the second test campaign the beam scan system was not used because the thruster always fired in alternate polarity.

However an indirect measurement of the horizontal beam divergence half-angle ( $\beta$ ) was obtained by the beam trace on the target, see Figure 50.

The horizontal beam divergence half-angle ( $\beta$ ) is

$$\beta = \text{atan}[l/(2d)]$$

where  $l$  is the trace width and  $d$  is the emitter-target distance. Since the width  $l$  is 330 mm and the distance  $d$  is about 780 mm, the  $\beta$  angle is close to 12 deg, confirming the value obtained in the first test campaign.

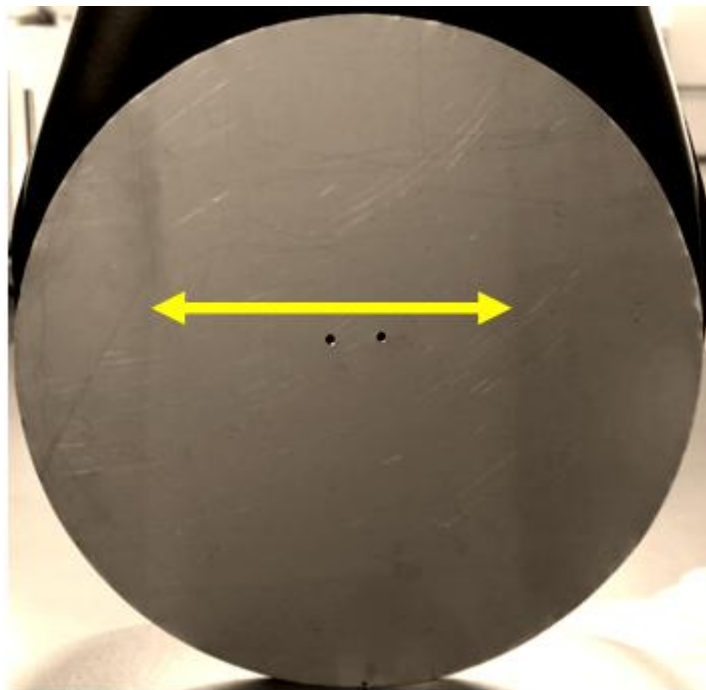


*Figure 50: Beam footprint on the metallic target*

### 6.4. Time of flight measurements

All measurements are carried out at a temperature of 27°C.

Figure 51 - Figure 54 show typical oscilloscope outputs with the time scale properly set to detect fast species (ions) in positive polarity mode. Measurements are carried out with the emitter voltage varying in the range +7.2 / +7.8 kV.

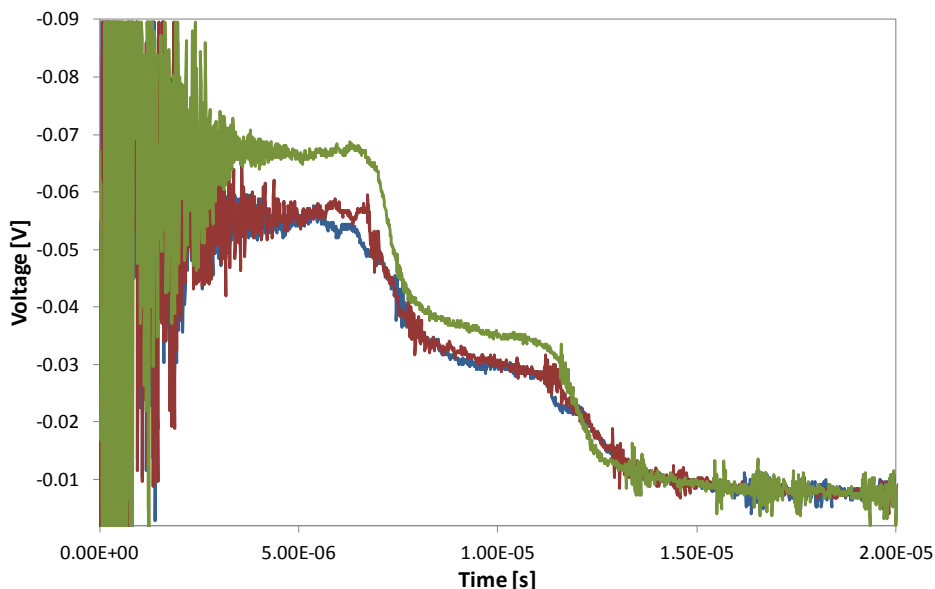


Figure 51: TOF measurements in positive polarity (+7.2 kV, 27°C)

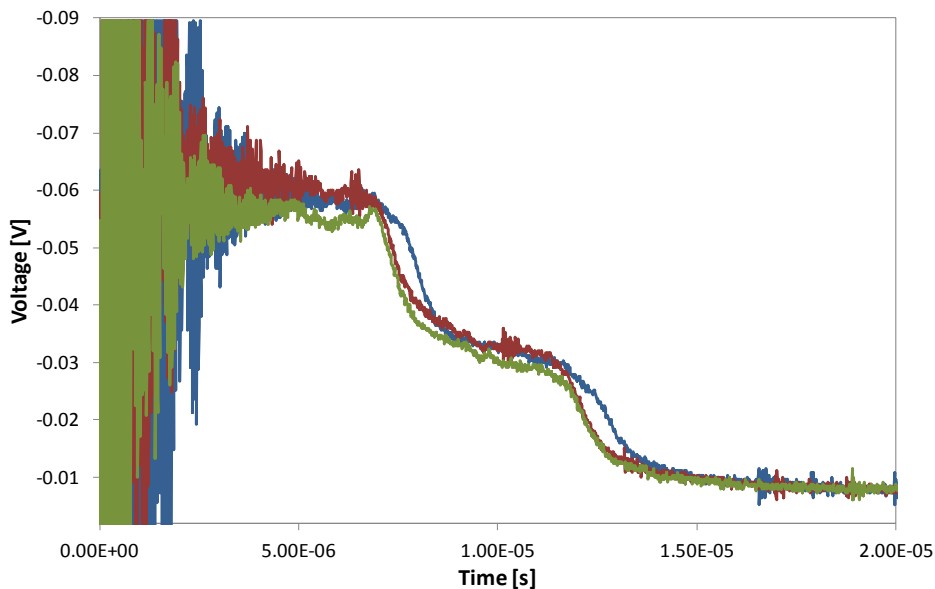


Figure 52: TOF measurements in positive polarity (+7.4 kV, 27°C)

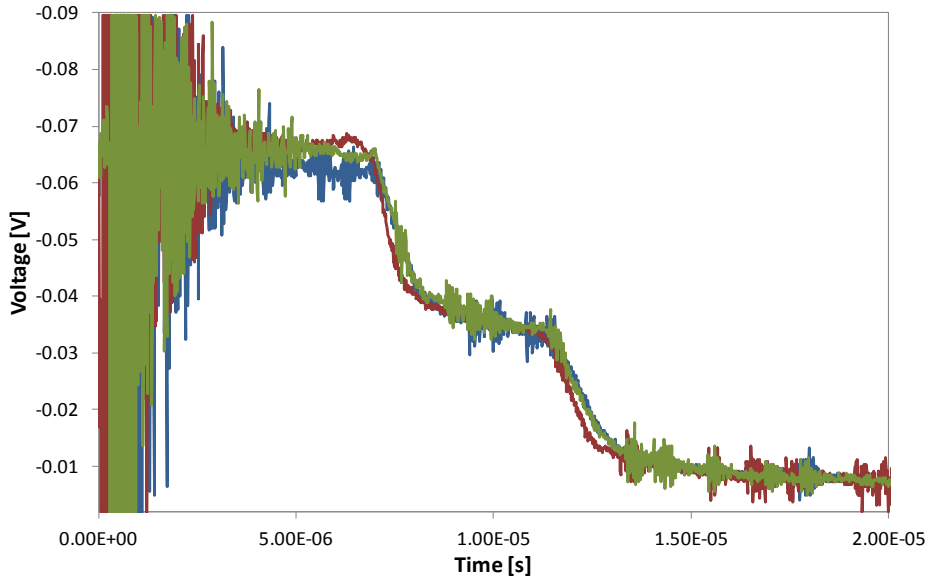


Figure 53: TOF measurements in positive polarity (+7.6 kV, 27°C)

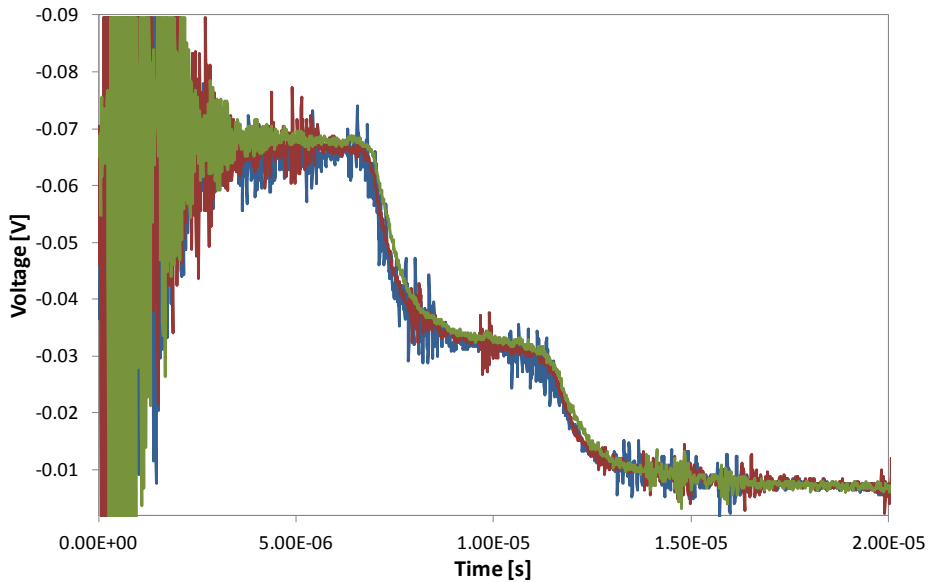


Figure 54: TOF measurements in positive polarity (+7.8 kV, 27°C)

Slope variations observed in the voltage plots are related with positive monomers and dimers, whose masses are 111.16 and 309.12 respectively. Table 4 summarizes the theoretical time of flight of monomers and dimers computed with the voltages used for the measurements. Experimental values of ToF match reasonably well the computed ones.

Voltage [kV]	Monomer ToF [s]	Dimer ToF [s]
7.2	6.98 E-6	11.63 E-6
7.4	6.88 E-6	11.48 E-6
7.6	6.79 E-6	11.32 E-6
7.8	6.70 E-6	11.18 E-6

Table 4: Theoretical ToF for monomers and dimers in positive polarity

Figure 55 - Figure 58 show typical oscilloscope outputs with the time scale properly set to detect fast species (ions) in negative polarity mode. Measurements are carried out with the emitter voltage varying in the range -6.9 / -7.6 kV.

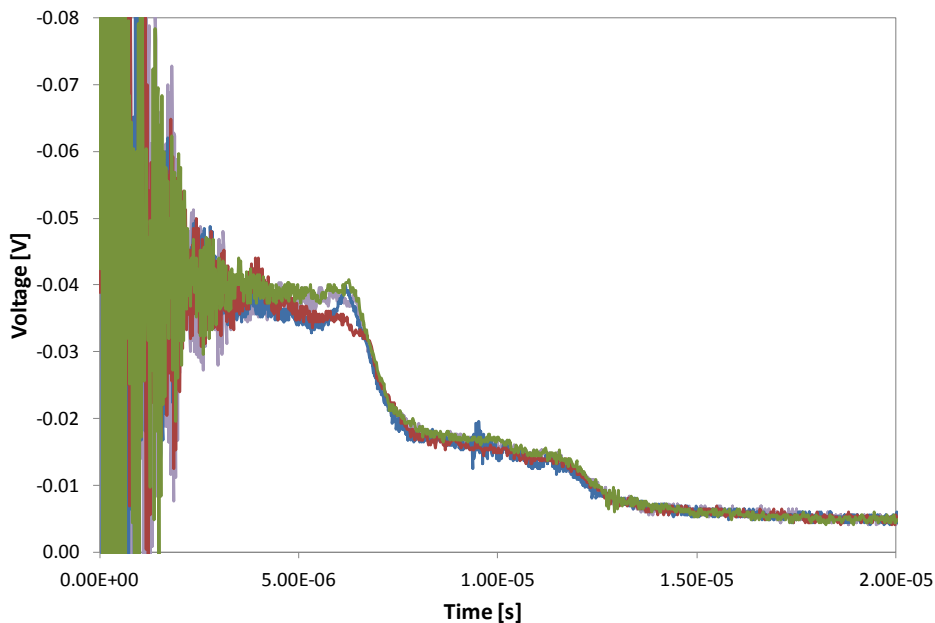


Figure 55: TOF measurements in negative polarity (-6.9 kV, 27°C)

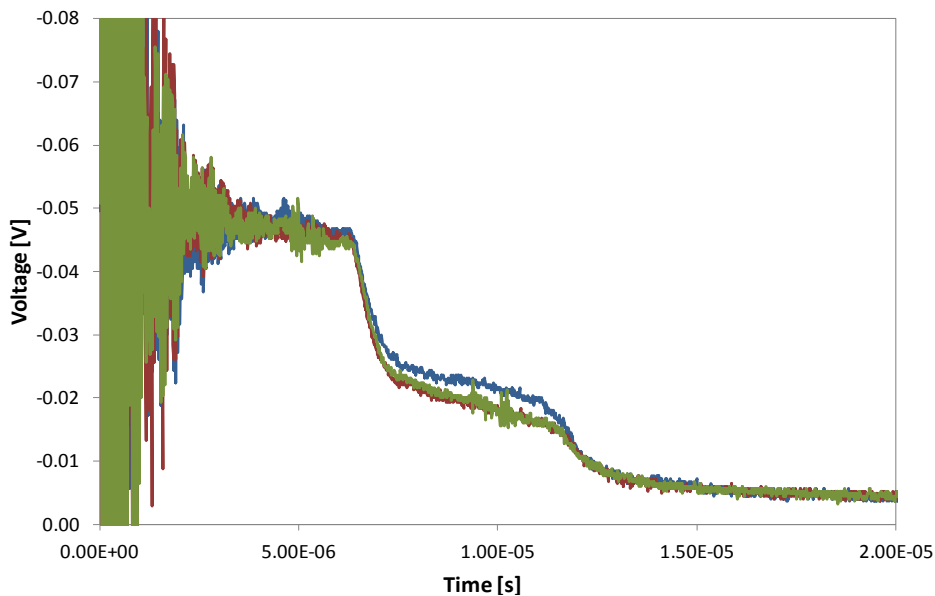


Figure 56: TOF measurements in negative polarity (-7.2 kV, 27°C)

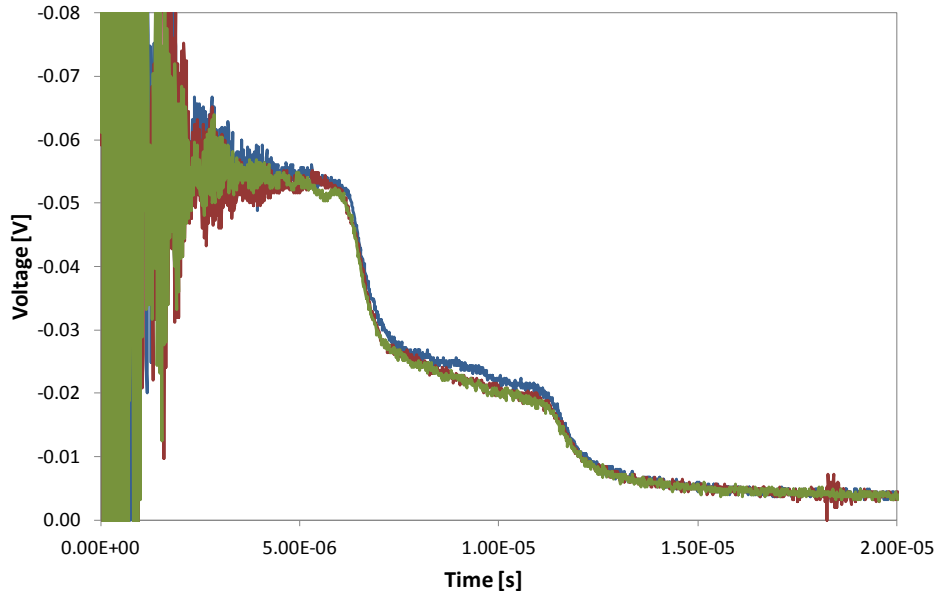


Figure 57: TOF measurements in negative polarity (-7.4 kV, 27°C)

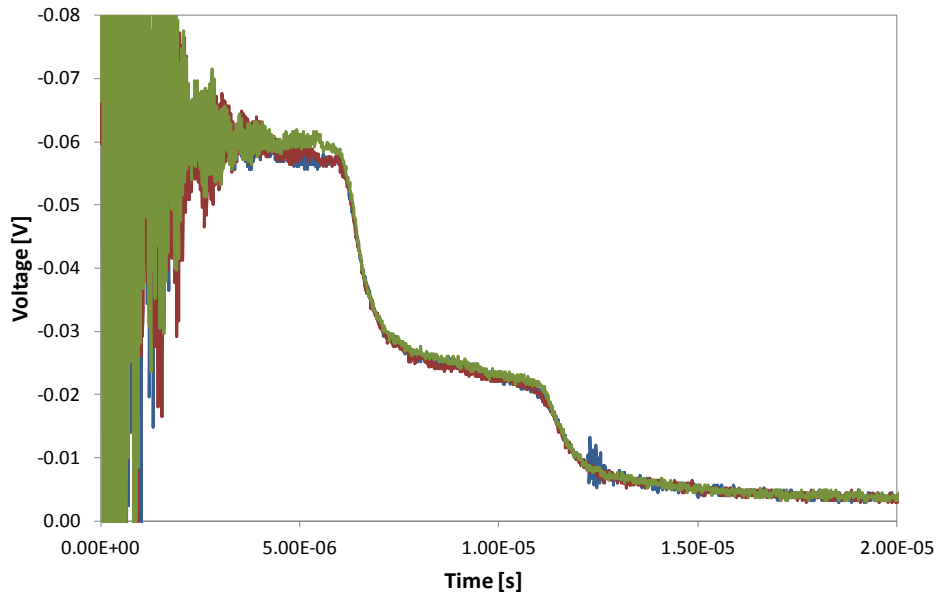


Figure 58: TOF measurements in negative polarity (-7.6 kV, 27°C)

Slope variations observed in the voltage plots are related with negative monomers and dimers, whose masses are 86.805 and 284.77 respectively. Table 5 summarizes the theoretical time of flight of monomers and dimers computed with the voltages used for the measurements. Experimental values of ToF match reasonably well the computed ones.

Voltage [kV]	Monomer ToF [s]	Dimer ToF [s]
6.2	7.52 E-6	12.54 E-6
6.9	7.13 E-6	11.88 E-6
7.2	6.98 E-6	11.63 E-6
7.4	6.88 E-6	11.48 E-6

Table 5: Theoretical ToF for monomers and dimers in negative polarity

A different time scale of the oscilloscope during acquisition allows for the detection of slow species that possibly compose the beam.

Figure 59 and Figure 60 show typical oscilloscope outputs with the time scale properly set to detect slow species (droplets) in positive polarity mode with +6.9 kV.

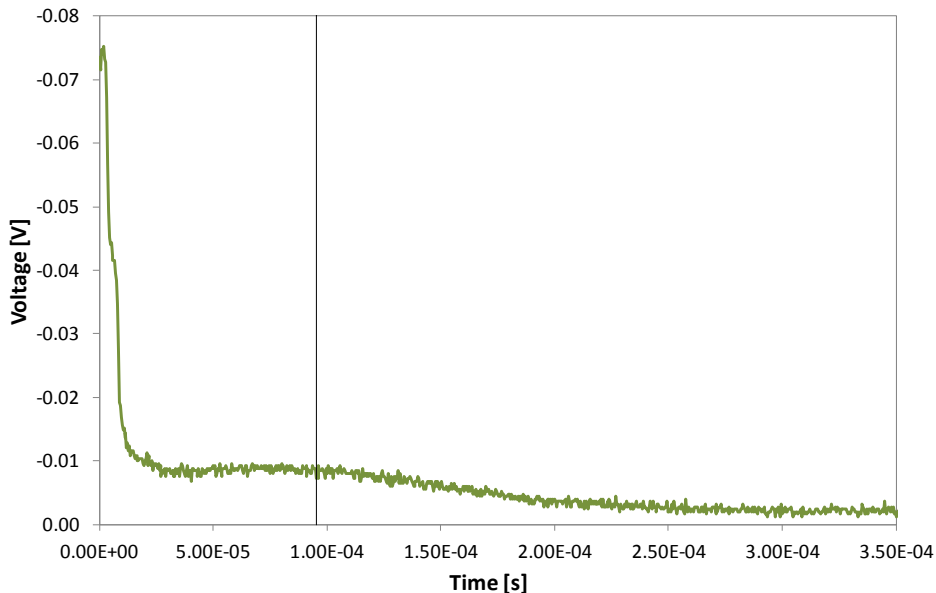


Figure 59: TOF measurement for detecting slow species (6.9 kV, 27°C)

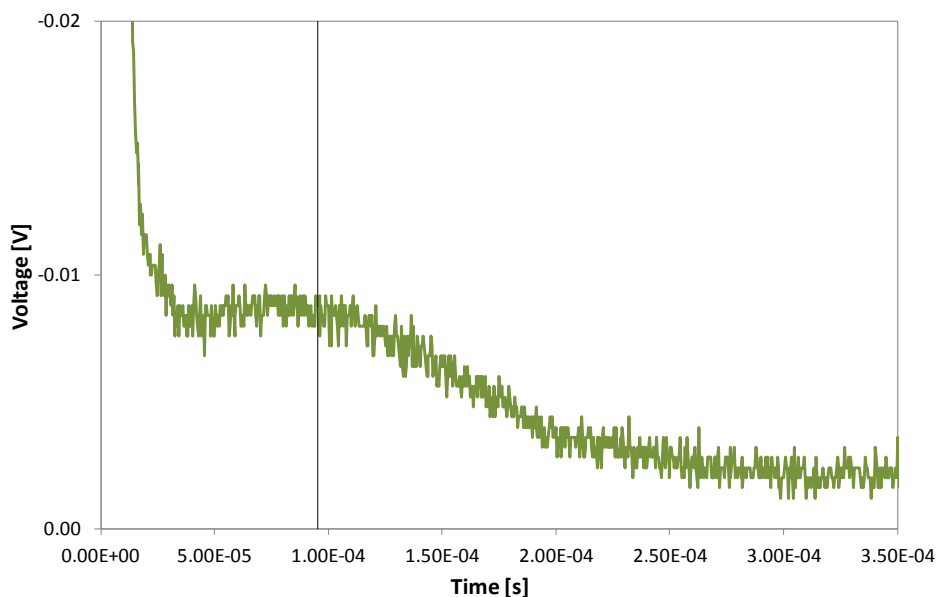


Figure 60: Close-up of Figure 59

According to Figure 60, the velocity of the slowest species is:

- $v = 0.78 \text{ m} / 9.5 \cdot 10^{-5} \text{ s} = 8,210 \text{ m/s}$ .

The corresponding mass-to-charge ratio is:

- $m/q = 2 V_e / v^2 = 13.8 \cdot 10^3 \text{ V} / (8,210 \text{ m/s})^2 = 2.05 \cdot 10^{-4} \text{ kg/C}$ .

Assuming only single charge species, the molecular mass is:

- $M = 2.05 \cdot 10^{-4} \text{ kg/C} \cdot 1.6 \cdot 10^{-19} \text{ C} / 1.66 \cdot 10^{-27} \text{ kg} = 197.6$ .

This means a number of molecules in a single droplet approximately equal to

- $N_{\text{droplets}} = 1973.1 / (111.16 + 86.805) = 99.8$ .

Figure 59 and Figure 60 show typical oscilloscope outputs with the time scale properly set to detect slow species (droplets) in positive polarity mode with +7.2 kV.

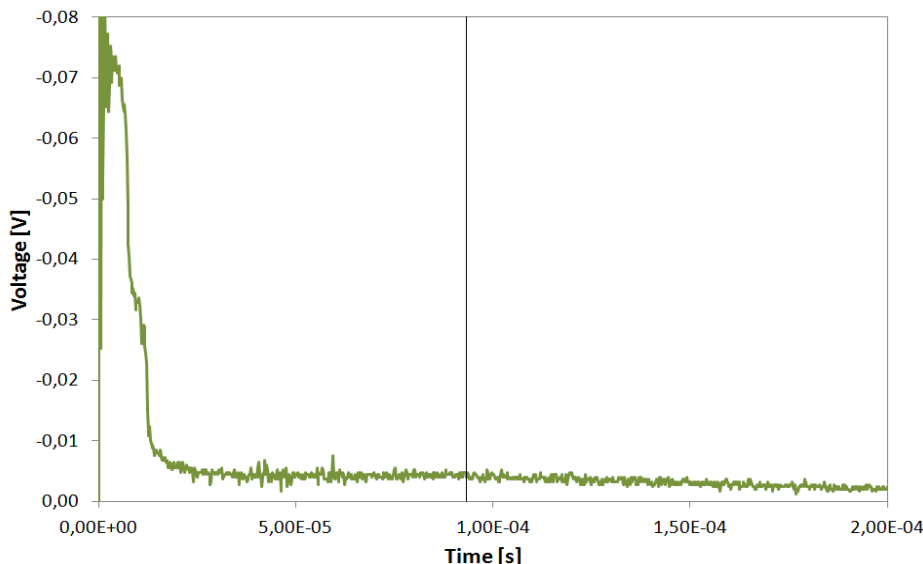


Figure 61: TOF measurement for detecting slow species (7.2 kV, 27°C)

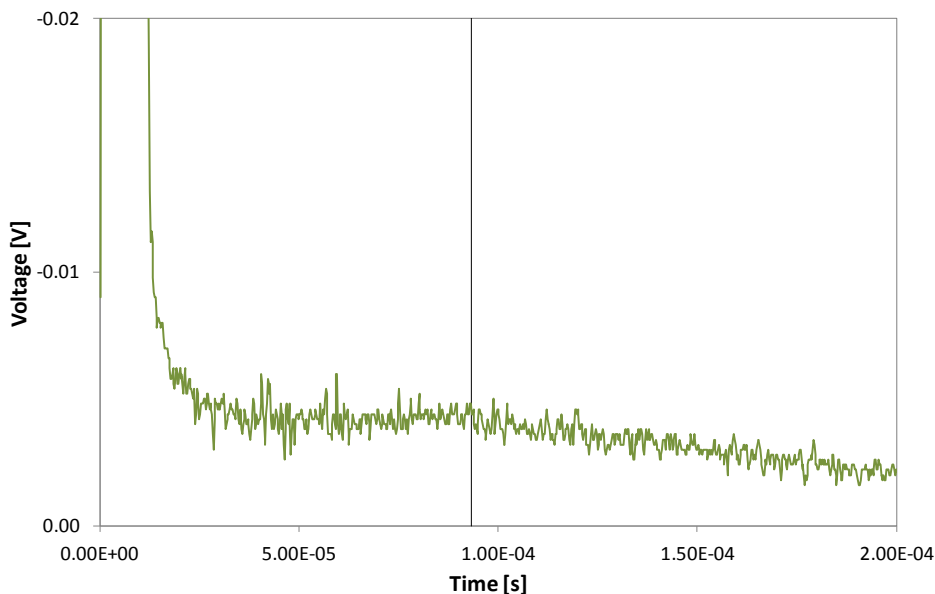


Figure 62: Close-up of Figure 61

According to Figure 60, the velocity of the slowest species is:

- $v = 0.78 \text{ m} / 9.3 \cdot 10^{-5} \text{ s} = 8387 \text{ m/s}$ .

The corresponding mass-to-charge ratio is:

- $m/q = 2 V_e / v^2 = 14.4 \cdot 10^3 \text{ V} / (8387 \text{ m/s})^2 = 2.04 \cdot 10^{-4} \text{ kg/C}$ .

Assuming only single charge species, the molecular mass is:

- $M = 2.04 \cdot 10^{-4} \text{ kg/C} \cdot 1.6 \cdot 10^{-19} \text{ C} / 1.66 \cdot 10^{-27} \text{ kg} = 196.6$ .

This means a number of molecules in a single droplet approximately equal to

- $N_{\text{droplets}} = 197 / (111.16 + 86.805) = 99.3$ .

Similar results were obtained with measurements carried out by varying the acceleration voltage between 6 and 8 kV, both in positive and negative polarity mode.

The results show that the beam is mainly composed of monomers and dimers, but also of a spectrum of droplets, whose heaviest one is made up of one hundreds of EMI-BF<sub>4</sub> molecules.

From the relative contribution of monomers, dimers and droplets to the ToF output (see Figure 63 and Figure 64) the average data summarized in Table 6 and Table 7 can be obtained.

	Distance [m]	Molecular mass [amu]	Velocity [m/s]	Time [s]	Current fraction
(EMI) <sup>+</sup> (BF <sub>4</sub> ) <sup>-</sup>	0.78	111.16 86.805	109,445.0 123,850.5	7.13E-6 6.30E-6	0.573
(EMI-BF <sub>4</sub> )(EMI) <sup>+</sup> (EMI-BF <sub>4</sub> )(BF <sub>4</sub> ) <sup>-</sup>	0.78	309.125 284.77	65,630.1 68,379.1	1.19E-5 1.14E-5	0.369
100 (EMI-BF <sub>4</sub> )(EMI) <sup>+</sup> 100 (EMI-BF <sub>4</sub> )(BF <sub>4</sub> ) <sup>-</sup>	0.78	~ 19,900	~ 8,180	~ 9.54E-5	0.058

Table 6: Average data for 6.9 kV ToF measurements

	Distance [m]	Molecular mass [amu]	Velocity [m/s]	Time [s]	Current fraction
(EMI) <sup>+</sup> (BF <sub>4</sub> ) <sup>-</sup>	0.78	111.16 86.805	111,798.9 126,514.3	6.98E-6 6.17E-6	0.541
(EMI-BF <sub>4</sub> )(EMI) <sup>+</sup> (EMI-BF <sub>4</sub> )(BF <sub>4</sub> ) <sup>-</sup>	0.78	309.125 284.77	67,041.7 69,849.7	1.16E-5 1.12E-5	0.368
100 (EMI-BF <sub>4</sub> )(EMI) <sup>+</sup> 100 (EMI-BF <sub>4</sub> )(BF <sub>4</sub> ) <sup>-</sup>	0.78	~ 19,900	~ 8,350	~ 9.34E-5	0.091

Table 7: Average data for 7.2 kV ToF measurements

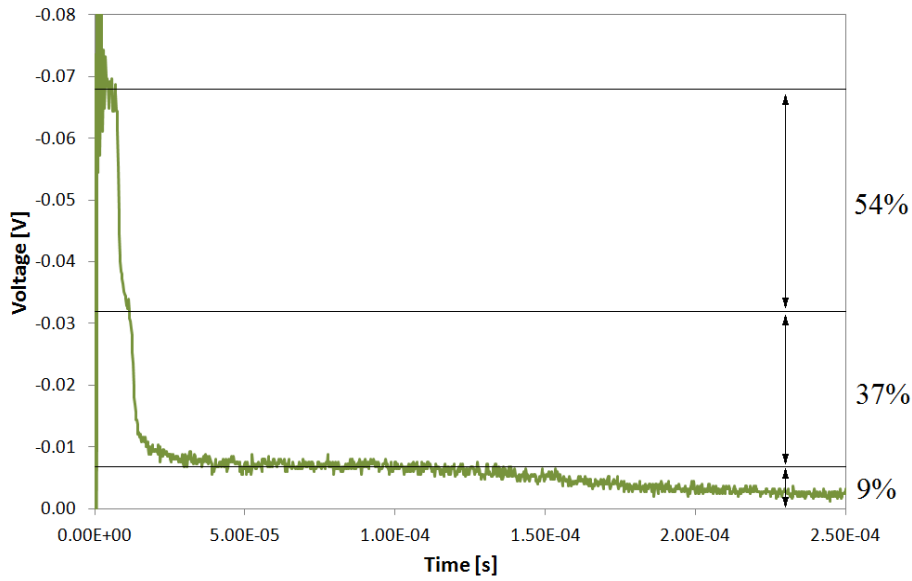


Figure 63: ToF output contribution of beam species (6.9 kV, 27°C)

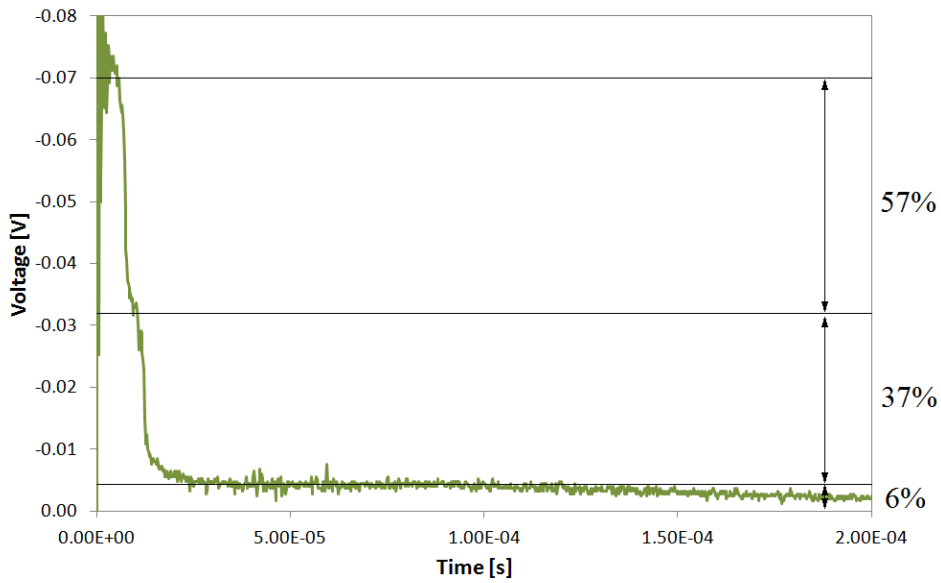


Figure 64: ToF output contribution of beam species (7.2 kV, 27°C)

### 6.5. Thruster performance estimation

From the beam current fraction, identified by ToF measurements, the mass flow rate of the each beam species is

$$\dot{m}_i = \sum_i \frac{\alpha_i I}{\frac{q}{m_i}}$$

where  $I$  is the beam current,  $\alpha_i$  and  $m_i$  are the beam current fraction and the mass of the  $i$ -th species and  $q$  is the elementary charge.

The total mass flow rate and the thrust are

$$\dot{m}_{\text{tot}} = \sum_i \dot{m}_i \quad T = \sum_i \dot{m}_i v_i$$

where  $\dot{m}_i$  and  $v_i$  is the mass flow rate and the velocity of the  $i$ -th species.

The specific impulse is

$$I_{sp} = \frac{T}{g_0 \dot{m}_{\text{tot}}}$$

where  $g_0$  is the Earth gravity acceleration.

The summation involved in these computations would be extended on all species composing the beam. Using ToF data the index  $i$  takes values 1, 2 and 3 to identify monomers, dimers and droplets (with N=100 EMI-BF<sub>4</sub> molecules) respectively.

Table 8 and Table 9 summaries these computations for a range of operating conditions.

Emitter Temperature [°C]	Emitter Voltage [kV]	Beam current [uA]	Mass flow [mg/s]	Thrust [μN]	I <sub>sp</sub> [s]
110	8.2	180	2.93E-03	52.3	1821
	7.5	70	1.14E-03	19.5	1741
	6.9	50	8.14E-04	13.3	1670
83	6.0	25	4.07E-04	6.2	1557
70	6.7	30	4.88E-04	7.9	1646
60	6.4	18	2.93E-04	4.6	1608
27	6.7	15	2.44E-04	3.9	1646

Table 8: Summary of thruster estimated performance in positive polarity

Emitter Temperature [°C]	Emitter Voltage [kV]	Beam current [uA]	Mass flow [mg/s]	Thrust [μN]	I <sub>sp</sub> [s]
110	8.4	200	3.20E-03	56.3	1792
	7.6	85	1.36E-03	22.8	1704
	6.9	60	9.61E-04	15.3	1624
83	6.2	30	4.81E-04	7.3	1539
70	6.9	40	6.41E-04	10.2	1624
60	6.6	25	4.01E-04	6.2	1588
27	6.7	20	3.20E-04	5.0	1600

Table 9: Summary of thruster estimated performance in negative polarity

The  $\alpha_i$  coefficients of the beam current contributions vary with the current emission (a larger contribution of droplets seems to be present in the beam at low emission currents). Data in Table 8 and Table 9 are estimated by using average values of the  $\alpha_i$  coefficients ( $\alpha_1=56\%$ ,  $\alpha_2=37\%$ ,  $\alpha_3=7\%$ ).

Performance estimation with discrete values of the  $i$  index entails an underestimation of  $I_{sp}$ , as contributions of different size droplets are entirely attributed to the larger and slower one.

## 6.6. Propellant consumption estimation

To verify the performance computations, the time variation of the propellant head was monitored during a sufficiently long firing time (27°C).

After a firing time of 120 h the propellant head decreased of about 3.9 mm. As the internal diameter of the duct is 5 mm and the EMI-BF4 density is 1218 kg/m<sup>3</sup>, it results an actual mass consumption of about 96 mg. The measurement is obtained by visual inspection of the propellant head level through the glass tube of the feeding system, see Figure 65.

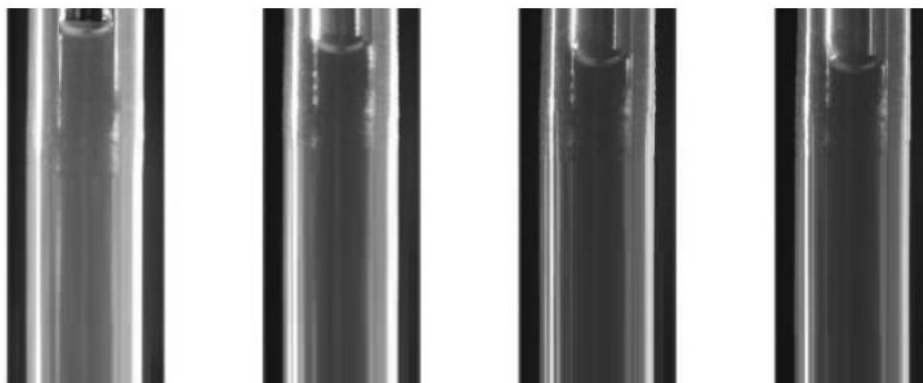


*Figure 65: Propellant head decrease during the 120 h period of firing time*

Computing the propellant mass usage from the theoretical mass flow rates (see Sec. 6.5) with the current and voltage levels used during the 120 h period, it results a mass consumption of about 105 mg (45.4 mg of positive ions and 59.3 mg of negative ions).

The difference between the two computations results to be about 9%. This difference may be ascribed to the uncertainty due to the visual inspection and to the conservative assumptions made in the specific impulse estimation via ToF results.